Effects on temporomandibular joint caused by orthodontic intermaxillary elastics

a finite element study

Inaugural-Dissertation

zur Erlangung des Doktorgrades

der Hohen Medizinischen Fakultät

der Rheinischen Friedrich-Wilhelms-Universität

Bonn

Yaqiu Zhang

aus Dalian/(PR) China

2022

Angefertigt mit Genehmigung der
Medizinischen Fakultät der Universität Bonn

1. Gutachter: Prof. Dr. rer. nat. Christoph Bourauel
2. Gutachterin: PD Dr. Pia-Merete Jervoe-Storm

Tag der Mündlichen Prüfung: 04.11.2022

Aus der Poliklinik für Zahnärztliche Prothetik, Propädeutik
Und Werkstoffwissenschaften der Universität Bonn
Direktor: Prof. Dr. med. dent. H. Stark
- Stiftungsprofessur für Oralmedizinische Technologie –
Prof. Dr. rer. nat. C. Bourauel

Table of contents

List of abbreviations

AC	Articular Cartilage
AD	Articular Disc
cbCT	cone beam Computed Tomography
FBi	Bite Force of Incisors
FBm	Bite Force of Molars
FE	Finite Element
FJ	Total Reaction Force of Joint
FM	Muscle Force of Masseter
FT	Muscle Force of Temporalis
MAL	Moment Arm Line
MaxPS	Maximum Principal Stress
Model ATT	Model with Anterior Teeth Traction
Model CII	Model with Angle's Class II Elastics
Model CIII	Model with Angle's Class III Elastics
Model CIIs	Model with Angle's Class II Short Elastics
Model CIIIs	Model with Angle's Class III Short Elastics
Model MT	Model with Molar Traction
Model VT	Model with Vertical Traction
Model WOOE	Model without Orthodontic Intermaxillary Elastics/Traction
OA	Osteoarthritis
OEs	Orthodontic Intermaxillary Elastics/Traction
OT	Orthodontic Treatment
TMD	Temporomandibular Joint Disorder

TMJ	Temporomandibular Joint
2D	Two Dimensional
3D	Three Dimensional
6DOF	6 Degrees of Freedom

1. Introduction

TMD (temporo-mandibular joint disorder) is a common musculoskeletal degenerative condition that is linked to several morphological and functional abnormalities. Although many epidemiological studies reported that TMD affects up to 25 % of the population, yet only a small percentage of the affected patients seek treatment (Murphy et al., 2013). Several classification schemes of TMDs are available and nearly most of them divide the TMDs into either muscular, articular or mixed disorders. TMD was first proposed as an oral disease in 1921 by Dr Gysi (Gysi, 1921). While in 1934, otolaryngologist James Costen presented “Costen syndrome”, which was the first evidence that related TMD and abnormal occlusions to other medical conditions such as hearing loss, vertigo, headache, etc. (Costen, 1997).

The so-called multifactorial aetiological theory of TMD is currently well accepted by many scientists and researchers, with the occlusion factor being one of the crucial aetiological causes. In the late 1980s, therapeutic approaches that were used to modify malocclusion or even facial growth patterns were thoroughly investigated. This happened especially after a lawsuit was able to prove that orthodontic interventions were the main cause of patient’s pain (Pollack, 1988). Moreover, many studies and reviews nowadays are quite concerned with the relationship between TMD and malocclusion or orthodontic treatment, because the aetiology and progression of the disease are poorly understood (Chisnoiu et al., 2015). Thus, the role of malocclusion in the aetiology of TMD is still controversial.

The relation between orthodontic treatment and TMD is studied using different approaches including animal, clinical, numerical studies (e.g.finite element method), and systematic reviews. With the help of the progressive evolution in computer science field, the finite element (FE) method is now considered one of the reliable methods with over 6-decade development to study biomechanics of the human body. The FE method has the advantages of reducing the expenditure of in vivo and in vitro studies, strictly controlling the variables, excluding the interfering factors, etc. (Hasan et al., 2012). Although, the FE model parameters are greatly based on the test results of human or animal studies, the computational result has a certain extent of meaning to the clinical practice (Sagl et al., 2019). In the following sections, we will discuss the temporomandibular joint (TMJ), TMD,

the relation between TMD and orthodontic treatment, and the application of computer methods in TMD investigations.

1.1 Temporomandibular Joint

1.1.1 The anatomy of the temporomandibular joint

The temporomandibular joint (Figure 1) is formed of two skeletal structures, the temporal bone (the glenoid fossa of the temporal squamous portion) and the mandible (mandibular condyle). The surfaces of the two skeletal structures are both covered by a thin layer of cartilage, which is 0.3-0.5 mm in thickness (Hasson et al., 1997). Similar to the knee, a biconcave articular disc (AC) is located between the convex mandibular condyle and the concave glenoid fossa to dissipate the bony load. The AC divides the space between the glenoid fossa and condyle into superior and inferior compartments. Moreover, the space is filled with synovial fluid, which helps with the lubrication of the joint and supplies nutrition to the avascular cartilaginous tissues (Herring et al., 2002; Okeson, 1998).

The disc is also surrounded by ligaments and muscles that control its movement and prevent disc dislocation. The disc is attached by discal ligaments (also known as collateral ligaments) to the medial and lateral pole of the condyle and is able to rotate from the front to the top of the condyle. The anterior side of the disc is connected to a portion of the superior lateral pterygoid, which can displace the disc forward. On the posterior side of the disc, there is superior retrodiscal lamina which binds the disc to the temporal bone.

The articular capsule originates from the border of the glenoid fossa, encloses the articular tubercle, and inserts at the neck of the condyle. There are three main ligaments located on each side of the mandible to support its function. The first one is the temporomandibular ligament, which is located on the lateral aspect of the capsule, preventing the lateral or posterior displacement of the condyle. The second one is the stylomandibular ligament, which starts from the styloid process and is attached to the mandibular angle. The former ligament limits the excessive protrusion of the mandible. The sphenomandibular ligament, which is the third ligament that runs between the spine of the sphenoid bone and the mandibular lingula and restricts the inferior movement of the mandible.

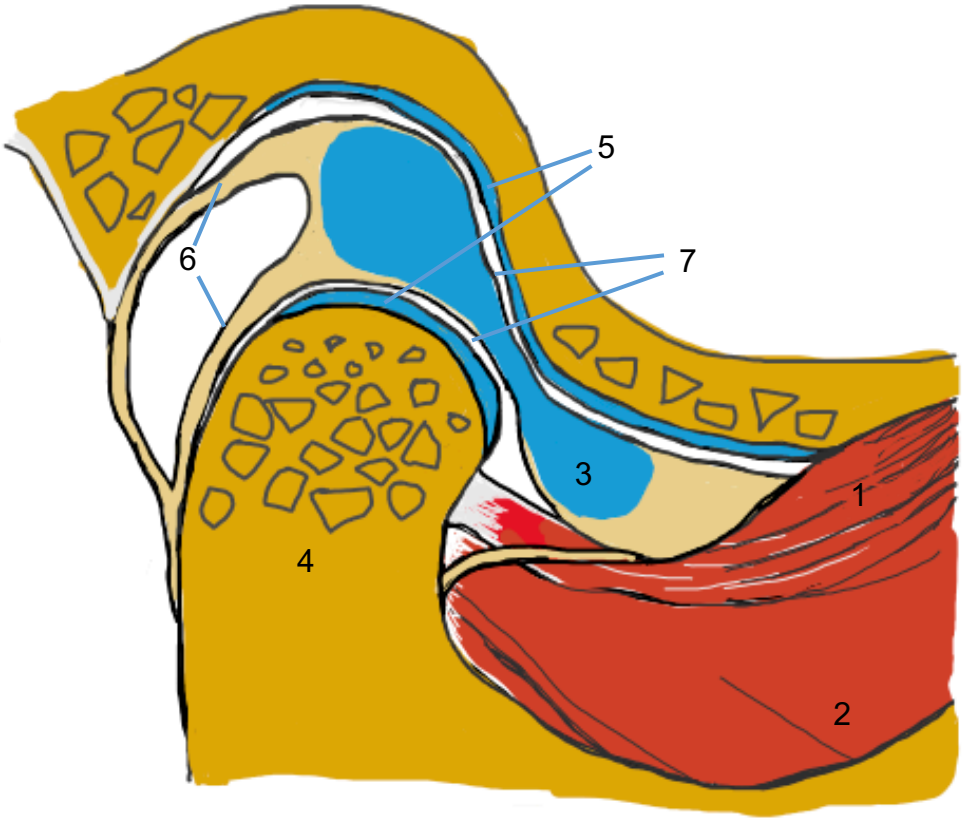

Figure 1: Lateral view of cross-section through the TMJ. I. Superior lateral pterygoid muscle; 2. Inferior lateral pterygoid muscle; 3. Disc; 4. Condyle; 5. Cartilage; 6. Discal lamina; 7. Superior and inferior compartments (adapted from Dawson, 2007).

1.1.2 The function and biomechanics of the temporomandibular joint

The TMJ is one of the diarthrodial synovial joints in the human body and a main component of the human masticatory system. As a hinge joint, the TMJ has 6-degrees of freedom, and the bilateral TMJs normally function together. The structure of the TMJ is advantageous for rapid and smooth mandibular movements, allowing for depression, elevation, protrusion, retrusion, and medio- and laterotrusion of the mandible (Motzko et al., 2019; Tanaka and Koolstra, 2008).

The initial mouth opening (approx. 20-25 mm) consists primarily of a rotational movement around a horizontal axis, connecting both medial poles of the condyle. It takes place in the inferior compartment, i.e., between the AC and the condyle. The intermediate mouth opening (approx. 20-35 mm) is a translational sliding movement of the condyle ventrally and caudally under the articular eminence. This movement takes place mainly in the superior compartment, i.e., between the AC and the mandibular fossa of the temporal bone

(Motzko et al., 2019). The terminal opening of the mouth occurs by tension of the lateral ligament. In addition, the passive forces of the elevator muscles control and limit the mouth opening.

Investigations of the biomechanics of TMJ started in 1980 and continued until it is proved now through numerous experimental and model studies that the TMJ is loaded during mandibular function in macaque (Boyd et al., 1990; Brehnan et al., 1981; Hylander and Bays, 1979) or human studies (Hatcher et al., 1986; Smith et al., 1986; Throckmorton and Dechow, 1994). It is established as well that the mechanical loading of the TMJ is essential for stabilization of occlusion and preservation of the living tissues of the mandible. This takes place through remodelling process, which is an important biological response to general functional stresses. However, excessive or sustained mechanical stresses can lead to stimulation of ossification and resorption of the TMJ, further leading to degradation and deterioration of the joint (Owtad et al., 2013).

The TMJ has highly irregular articular surface with a very small contact area that is not covered by cartilaginous tissues, leading to high peak loads and friction. The synchronisation between the AC and the articular disc plays a crucial role in TMJ function, which is believed to distribute the stresses and shield the underlying bone (Detamore and Athanasiou, 2003; Singh and Detamore, 2008; Tanaka et al., 2006). The condylar cartilage consists of several layers, which are the fibro cartilaginous fibrous, proliferative, mature, and hypertrophic zone (Luder et al., 1988; Mizoguchi et al., 1996). The different layers contain different types of collagen fibres, and among them, type I collagen that differs from the cartilage of other joints.

The three-dimensional collagen network is arranged along the anteroposterior direction, stabilizing the cartilage form, and provides tensile strength and resistance against shear forces (Hayes and Bodine, 1978; Singh and Detamore, 2008; Wang et al., 2009). The collagen matrix has a very low permeability, leading to the viscoelastic properties of the cartilage (Mow et al., 1993). Another important component of condylar cartilage matrix is the proteoglycans that contribute to resistance to compression (Mao et al., 1998; Stegenga et al., 1991). Furthermore, the fibrocartilage of the TMJ is avascular, and nourished mainly by the intro-articular synovial fluid (Aoyama et al., 2004).

Generally, there are three kinds of fundamental loadings of the joint: compression, tension, and shear (Kuroda et al., 2009). The deformation and internal forces of the cartilage

are also known as strain and stress. These two mechanical features depend on the components of the condylar cartilage, which behave nonlinearly, viscoelastically, and anisotropically. The tensile strength, tensile stiffness, and energy absorption in the anteroposterior direction are averagely larger than that of the mediolateral direction. The dynamic elastic modulus is significantly larger than the dynamic viscous modulus, and the moduli in the anterior area of cartilage are significantly larger than those in the posterior area.
The TMJ disc, similar to articular cartilage, is also a fibrocartilaginous tissue, which is composed of a unique matrix of collagen and cell phenotype. The human TMJ disc contains a large amount of water (74.5 % by wet weight), collagen (62.0 % by dry weight), and a small amount of glycosaminoglycan (3.2 % by dry weight; Kuo et al., 2010). Kuo et al. found that the average equilibrium moduli of the intermediate, lateral, and medial parts of the disc were statistically higher than the anterior and posterior ones (Kuo et al., 2010). TMJ disc has a biphasic viscoelastic (poroelastic) property owing to its liquid content. The collagen network impedes fluid flow through it instantly after the loading occurs. Thus, when the hydrated disc is subjected to dynamic compression with a loading frequency that is higher than the characteristic frequency of the tissue, the tissue will become stiffer (Soltz and Ateshian, 1998). However, with time, fluids are driven away through pores in the collagen network due to loading (Scapino et al., 1996). This phenomenon is responsible for the time-dependent biomechanical behaviour of the poroelastic property.

1.2 TMD and orthodontics

Temporomandibular disorders were defined as an umbrella term by the American Academy of Orofacial Pain, covering a series of musculoskeletal and neuromuscular conditions (de Leeuw, 2018; Valesan et al., 2021). Nowadays most scientists and researchers believe that TMD is a result of multiple direct or indirect factors (Michelotti and Iodice, 2010). The aetiological risk factors of TMD include age, genetic factors, sex, occlusion, hyperlaxity, parafunctional habits, trauma, bruxism, psychological factors, and orthodontic treatment (Roda et al., 2008a). As malocclusion is considered one of the main causative factors for TMD (de Leeuw, 2008), several studies focus on the relationship between TMD and orthodontic intervention. (Luther, 2007; Michelotti and Iodice, 2010).
Orthodontic intermaxillary elastics or traction (OEs) are widely used in orthodontic treatment to normalise the sagittal, vertical, and transversal occlusal relationships, by applying

tensile forces. According to the therapeutic plan, OEs can be applied between the maxilla and mandible either on the bracket of corresponding teeth or the added hook on the arch, or the mini-implant. As the mandible is a main part of the TMJ, the applied load can always be transferred from the teeth and alveolar bone to the TMJ and vice versa. Due to the sensitivity of AC to the alteration of the surrounding biomechanical environment, OEs might lead to remodelling of TMJ (Breitner, 1940; de Clerck, et al., 2012; Gurbanov et al., 2020).

1.2.1 Clinical studies of the relation between TMD and OEs

Clinical investigations of the possible links between orthodontic treatment and TMJ usually involve reporting symptoms and/or signs of TMD in treated and untreated, patients, different treatment methods, and comparing joint spaces using radiological approaches (Al-Saleh et al., 2015; Luther, 2007). Most of these studies included patients with multiple types of malocclusions, thus the correlation between different therapeutic approaches and TMD cannot be exactly specified.

A prospective observational cohort study by Henrikson and Nilner (Henrikson and Nilner, 2002) is one of the very few studies with specific types of malocclusions. They compared two groups of subjects with Class II division 1 malocclusion with a group of subjects with normal occlusion. All the subjects were females in the age range of 11-15 years old. Class II OEs were applied to the treated group. The symptoms and signs of TMD of the subjects were examined at the start and after 2 years for all the groups. For the treated group, additional follow up was performed 1 year later after the active treatment. In this study, the Research Diagnostic Criteria were adopted, which are one of the most valid and reproducible assessment indices of TMD (Dibbets and van der Weele, 1992). They found that although the subjects in all the groups showed increased or fewer signs and symptoms of TMD, the normal group had the lowest prevalence of TMD. The prevalence of TMD in the orthodontic treated group was significantly less than the untreated group. But Luther et al. (2007) did not agree that the study design could lead to such conclusions, and that the authors were not to exclude other explanatory factors.

A radiographic study by de Clerk et al. (2012) confirmed the remodelling of the TMJ in patients (9-13 years old) undergoing Class III OEs treatment. The applied traction force started with 1.5 N on each side, and it was increased to 2.0 N after one month, then to 2.5

N after three months traction. All the patients were imaged with cone-beam computed tomography (cbCT) before and after the OT. With the help of 3D models generated from the cbCT images, obvious posterior displacement of the whole mandible (ramus, condyles, and chin) was seen in all the subjects. Moreover, most of the patients showed remodelling signs and bone resorption of the anterior eminence. However, one limitation of this study is that the researchers did not consider the condition of TMJ of all the patients before and after the OT.

1.2.2 Animal studies of the relation between TMD and OEs

An animal study from Breitner (Breitner, 1940) assessed the effect of OEs on different areas of the mandible and TMJ. Macacus rhesus monkeys were included in the animal OT model, and Class II and Class III OEs were applied. After 82 days of traction, the monkeys were sacrificed, and histological specimens were prepared and examined. The researchers found not only resorption and deposition in the glenoid fossa and condylar head but also changes in the mandibular angle and alveolar processes. Results showed that with Class II OEs, the resorption occurred at the posterior edge of the mandibular angle, while deposition of new bone was found at the anterior margin, which indicated the widening of the angel. A slight mesial movement of the lower teeth was observed, while the evidence of the distal movement of the upper teeth was not significant, changes were found at the mandibular angle of the subject with Class III OEs, which indicated that the angle was becoming more acute.

Xu et al. in 2009, found that asymmetric OEs influenced the expression of the RANKL-OPG system in the condylar subchondral bone of adult rat. In this study, 160 rats, three months old, were included, and divided into three groups. The experimental groups were subjected to unilateral elastic traction, and the initial elastic forces were 0.4 N and 1.2 N. After 28 days of traction, the expression of OPG protein was equal in all the treated groups. While the expression of RANKL protein was stronger in the 1.2 N group compared to the 0.4 N group. This study showed that different intermaxillary traction forces regulate remodelling of adult TMJ. They accounted this to the expression of RANKL protein, which has the ability to co-regulate the functions of osteoblasts and osteoclasts in cartilaginous tissues of TMJ

1.2.3 FE method studies of the effect of OEs on TMJ

To evaluate the effects of OEs used in fixed orthodontic treatments on the TMJ, Gurbanov et al. developed four static FE models from two subjects, one with normal TMJ and the other with anterior located disc (Gurbanov et al., 2020). Then according to Angle's classification, four models were manually created as two skeletal Class II models and two skeletal Class III. Every model included both arches, TMJ disc, lower teeth with the periodontal ligament, and the fixed orthodontic applications. Linear material properties were applied to all the models. The articular cartilage (AC), discal ligament, and retrodical lamina were neglected in the study, and no muscle models were included. The contact in TMJ was simulated with gap elements and the frictional coefficient was 0.0001, and the contact relations of the left structures were all defined as "glue". The 2 N OE force was loaded on each side, and the configuration depended on Angel's classification. The numerical results showed that OEs in Class II models caused greater stress in the disc and condyle than in Class III models. They also concluded that OEs could be more dangerous to Class II patients with anterior located disc.

1.2.4 The theoretical mechanism

Proper loading of the TMJ is beneficial to maintain homeostasis of the joint, functional and occlusal relationships (Tanaka and Koolstra, 2008) as well as remodelling of the mandibular condyle. Alternatively, overloading of the joint might cause degenerative changes of the AC and subchondral bone, which may progress to osteoarthritis (OA) (Kuroda et al., 2009; Tanaka et al., 2008). At the early stage of joint remodelling, the tissues undergo hypertrophic repair to erase the symptoms and this phase can last for decades. However, as the load constantly surpasses the adaptation capacity of chondrocyte, insufficient production of the matrix occurs followed by collapsing of the AC and Synovitis.

During this fibrillation progress, the decrease of proteoglycans will cause softening and reduction of the thickness of the AC and vertical defects. In healthy TMJ patients, the coefficient of friction between the cartilage surfaces is approximately zero due to the presence of the synovial fluid (Tanaka et al., 2004), while the abrasion of the AC in OA can lead to 3.5 times greater coefficient of friction than that of the healthy joint. The shear stresses between the disc and the two ACs increase due to the rise of the friction coefficient. In this condition, the functional movement of the joints leads to fatigue and

irreversibly deforms the TMJ tissues with disappearance of the cartilage layer (Beatty et al., 2003; Tanaka et al., 2003). However, this whole process is hard to be examined radiologically as the indicative features of TMJ-OA cannot be correlated to the corresponding clinical symptoms until the exposed AC generate sclerosis in the subchondral region (Roda et al., 2008b).

1.3 Modelling of TMJ and masticatory system

Researchers began to explore the possibility of biomechanical modelling of TMJ with or without masticatory muscle kinetics using the advanced computer technology. It took over forty years, from the two-dimensional static models with extremely simplified structures to the development of three-dimensional dynamic sophisticated FE models. In this section, the finite element method, Hill-type muscle model and the published relating studies of other researchers will be discussed.

1.3.1 Modelling of the TMJ

Before the introduction of the first 3D FE model of TMJ with the mandible (Tanaka et al., 1994), TMJ models were typically oversimplified static 2D rigid or FE models (Haskell, 1986; Greaves, 1978; Throckmorton and Throckmorton, 1985). Furthermore, only one or two pairs of masticatory muscles were employed as two 2D force vectors, and the force magnitude was derived from the isometric biting force (see Figure 2).

In 1994, Tanaka et al. developed a 3D FE model of TMJ consisting of 2088 nodes and 1105 elements utilizing the ANSYS program. The model was based on a young human dry skull, which was sliced transversely into sections and each section was photographed. The photographs were then traced to drawings, and according to the anatomy were divided into meshes. Afterwards, they stacked all the meshed sections to a 3D structure of the model with constructed TMJ disc and cartilage. This is still a static model with components granted linear material properties. Six pairs of elevators were employed to simulate clenching in this study.

A basic dynamic 3D model of the masticatory system that simulated only elevator muscles and the jaw-closing movement was introduced in 1995 (Koolstra and van Eijden, 1995). Two years later, the same authors published a relatively more developed model with both

elevators and depressors to compare their mechanics during jaw movement (Koolstra and van Eijden, 1997). In this study, the mandible was characterised as a rigid mass with 6 degrees of freedom (6DOF). The condyle and the glenoid fossa were simplified as a sphere and a curvy surface respectively. The contacts between the articular structures and the two jaws were assumed as purely elastic and frictionless. Although the model has an oversimplified anatomy and even the material properties were neglected, it involved a muscle model which drives the movement of the mandible.

In 2005, a dynamic model of the human masticatory system with combination of coarse rigid skeletal structures and FE cartilaginous tissues was constructed for the first time. (Koolstra and van Eijden, 2005). The mandible was motivated by 12 pairs of muscles, including elevators and depressors, which were described as Hill-type activators. Moreover, the disc and cartilage were approximated as Mooney-Rivlin hyperplastic material

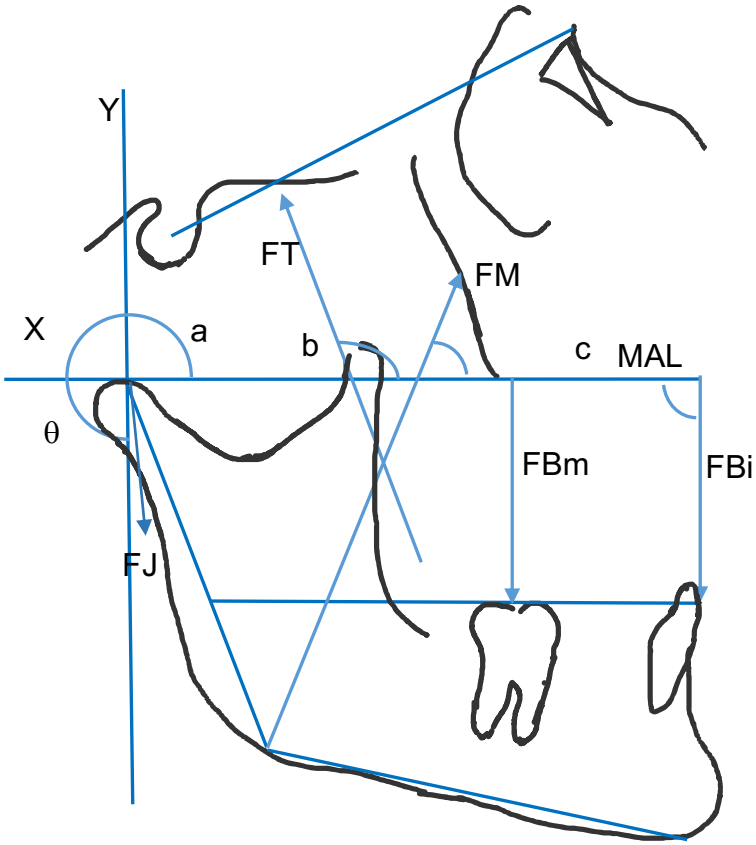

Figure 2: A basic 2D model of the TMJ. Muscle force of temporalis (FT); muscle force of masseter (FM); total joint reaction force (FJ); bite force of molars (FBm); bite force of incisors (FBi); moment arm line (MAL); a, b, c are the moment arms of FT, FM and FJ; θ is the angle between FJ and MAL (adapted from Throckmorton and Throckmorton, 1985).

models. While the TMJ model of this study was constructed from the right joint of one cadaver, and the left one was formed as a mirror image. Face asymmetries, which are quite common in humans, were ignored.

Based on the former study, Sagl et al. developed a dynamic rigid-FE combined model from CT and MRI data using an open resource program (Sagl et al., 2019). Clenching, protrusion and opening were simulated and compared with the data on the mandibular and disc movement of the subject. In addition, Commiso et al. (Commiso et al., 2014) created another model with more complex materials, which was closer to the cartilaginous nature of the human body. Since the purpose of that study was to assess the effect of the bruxism on TMJ, the isometrical muscle force was applied as external load respectively at the muscle insertion area to mimic a sustained clenching and a rhythmic masticatory muscular activity. For the cartilaginous structures, they used a quasi-linear viscoelastic material model, which is approximated by the relaxation function. In this function, the stress was decided by time, stretch and the elastic response.

1.3.2 Finite element method

The term “finite element” is derived from the direct analogy of the engineering view. FE analysis is a method of approximation to continuum problems, in which the continuum is divided into a limited (finite) number of components (elements) with specified behaviour. For the complete system, the rules applicable to discrete problems are the same as those for an assembly of its elements. Originally, the FE method, as a numerical solution is popular in engineering and mathematical modelling. It is traditionally practiced in structural analysis, heat transfer, fluid flow, etc. (Klein, 2012).

FE method or analysis contains three basic procedures: preprocessing, solver and post-processing (Meissner and Maurial, 2000). The entire FE analysis can be regarded as solving a system of equations according to the available parameters and algorithms. The preprocessing is to prepare this system of equations, including the development of the mesh of geometry, the application of the physical properties, and the definition of boundary conditions. After the preparation is accomplished, the whole system of equations (the FE model), will be submitted to the “solver” (computer) to calculate the result.

Once the simulation is finished, the results can be passed on to the postprocessing program and be shown in different forms according to the demand. For example, in Marc/

Mentat, the vectors can be shown as arrows in colours to indicate the direction and the magnitude of the value. FE methods are now widely used in the medical and dental field. By using the FE method, the financial consumption can be decreased compared to the in vivo or in vitro studies. It is also possible to reform the geometry of the subject, as well as changing the different parameters, which is much easier in comparison to the in vivo or in vitro conditions (Hasan et al., 2012).

1.3.3 Masticatory muscle and Hill-type muscle model

The jaw movements are controlled by three masticatory muscles, which are the elevators, depressors and lateral pterygoid muscles. The elevators are masseter, temporalis and medial pterygoid muscles. The depressors include geniohyoid, mylohyoid, and anterior digastric muscles. The elevators respectively originate from the zygomatic, temporal bone and medial pterygoid plate. The masseter and medial pterygoid muscles insert into the mandibular angle and inferior and superior area around it. Moreover, the temporalis muscle inserts into the coronoid process.

The depressors originate from the floor of the mouth, connecting the hyoid bone and the mandibular body. The lateral pterygoid contains two heads originating from the lateral pterygoid plate. The superior head inserts into the articular capsule, disc and condylar neck and is responsible for mouth closure. The inferior head is inserted into the condylar neck and allows the condyle to achieve a large mouth gap during mouth opening (Ash and Nelson, 2010, Hiraba et al., 2000).

The masticatory muscle forces are classified into passive and active forces. They both depend on the optimum isometric force and the muscle length, while active force also depends on the contracting velocity and the activation levels. To express the biomechanical behaviour of the skeletal muscle, a mathematical muscle model was proposed which included three elements (see Figure 3): the contract element (CE), the series element (SE) and the parallel element (PE) (Hill, 1938; 1953; Martins et al., 1998; Vilimek, 2007, Winters and Stark, 1987).

CE represents the active muscle force that is categorised as freely extensible when it is not activated, while it can get shorter when it is activated. SE is a nonlinear spring in series with CE, and it is capable of storing energy. SE permits the CE to switch rapidly from inactive to the active condition. PE is also a nonlinear spring paralleling CE and SE, which

expresses the passive muscle force when being extended. The muscle force-length and force-velocity behaviour are shown in Figure 4. This muscle model is widely used in studies of the masticatory system, including the investigations of muscular functions (Garcia et al., 2015; Langenbach and Hannam, 1999; Peck et al., 2000), biomechanic properties of TMJ and mandible (Koolstra and van Eijden, 2005; Sagl et al., 2019; Tuijt et al., 2010).

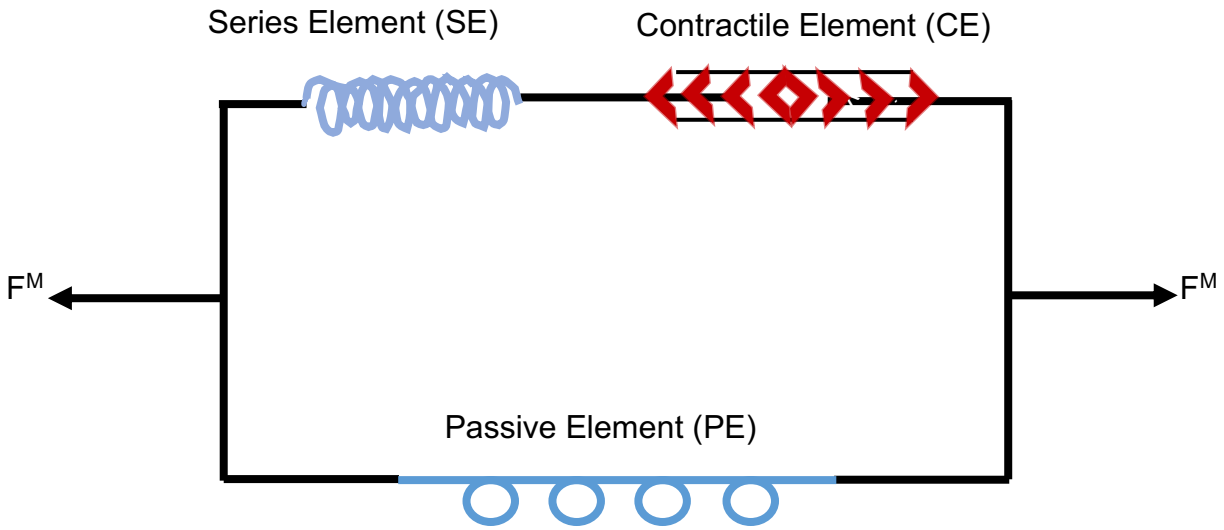

Figure 3: Hill type three-element muscle model (adapted from Martins et al., 1998).

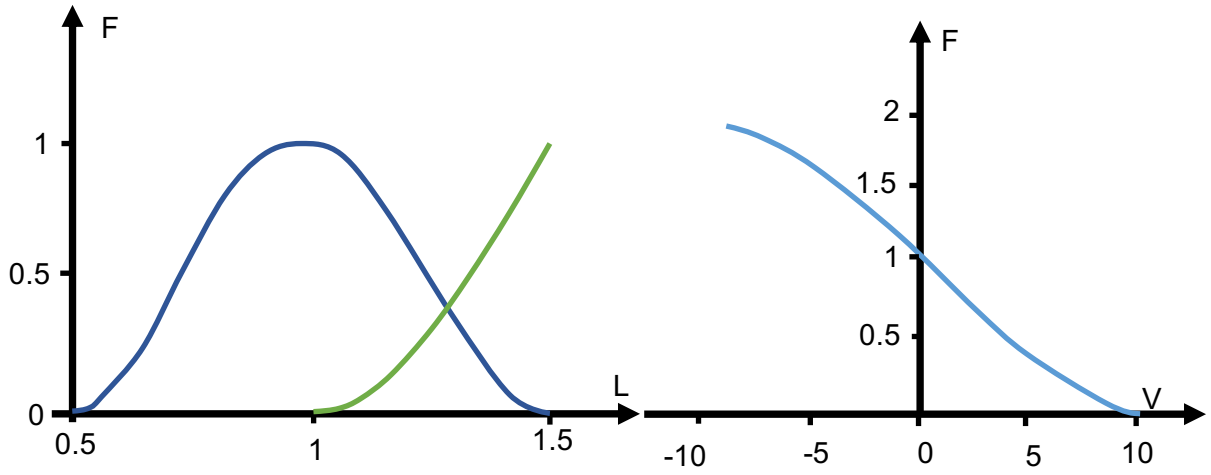

Figure 4: The muscle force-length and force-velocity behaviour (adapted from Langenbach and Hannam, 1999).

2. Aim

The purpose of the present study was to examine the biomechanical effect on TMJ caused by orthodontic intermaxillary elastics (OEs), using finite element (FE) methods. Since different configurations of OEs can apply different forms and magnitudes of forces on the TMJ, eight models, one reference model without elastics, and seven models with variations of OEs were developed. With the help of the FE method, the following questions were investigated:

- What is the biomechanical load in the TMJ during mouth opening and closing, including the magnitude and the distribution patterns?

- Compared with the model without elastics, will OEs cause excessive mechanical stresses in the healthy TMJ, and will the distribution pattern of the stress change?

- Will the OEs influence the trajectory of the mandible? If so, does it match the treatment aim?

3. Materials and methods

3.1 Generation of the 3D-mesh

A three-dimensional (3D) biomechanical TMJ model was built using Mimics 24.0, 3-Matic Research 16.0 and MSC.Marc/Mentat 2020. This TMJ model was driven by the masticatory system which was established according to the Hill muscle model (Hill, 1953). The modelling was performed on a desktop computer with a Windows 7 professional operating system, Intel Xeon E5-1620 v2 3.70GHz processor, 16.0 GB of random-access memory of the cluster. The simulation was performed on a Dell Server, which contains processors. The geometry of the model was based on the cbCT scan and MRI scan from an anonymised patient. This subject should meet the following inclusion criteria: 1. 14 years old or older (female), 16 years old or older (male); 2. individual normal occlusion; 3. no morphological abnormalities of TMJ. The age range was chosen according to the growth stage: The growth spurt starts in females around age 12, in males around age 14 and it usually slows down after two years (Proffit et al., 2013).

The mesh was prepared in Mimics and 3-Matic. DICOM (digital imaging and communications in medicine) files were imported into Mimics 24.0 and masks of skeletal parts were generated separately by specifying the maximum and minimum radiodensity values. Then the initial 3D model was exported into 3-Matic Research 16.0 for further refinement. The model was meshed in 3-Matic and divided into 5 parts including the cranium, cortical mandible, cancellous mandible and two discs. Every part consists of only one continuous closed surface mesh except for mandibular cortical bone (which should be hollow inside, so it has two surfaces, see Figure 5). Subsequently, we used fix wizard to detect failures and noise of the surface mesh; sharp apexes, unnecessary paths and chambers inside of the structures were discovered, eliminated and repaired to avoid numerical errors in the simulation. Afterwards, the whole model was remeshed to get a relative uniformly divided mesh. To reduce the computational consumption in the subsequent simulation, the glenoid fossa, the disc and the condyle were remeshed with higher mesh density. The teeth were remeshed with medium mesh density and the remaining structures were remeshed with low mesh density. Since the mandibular cortical bone should coincide with cancellous bone without bias, the inside surface of cortical bone should be the same as cancellous bone. Therefore, we removed the original inside surface of the cortical bone and used a

duplicated surface of cancellous bone instead of the original one. Finally, all the surface meshes (see Figures 5 and 6) of parts were exported as Abaqus files one by one.

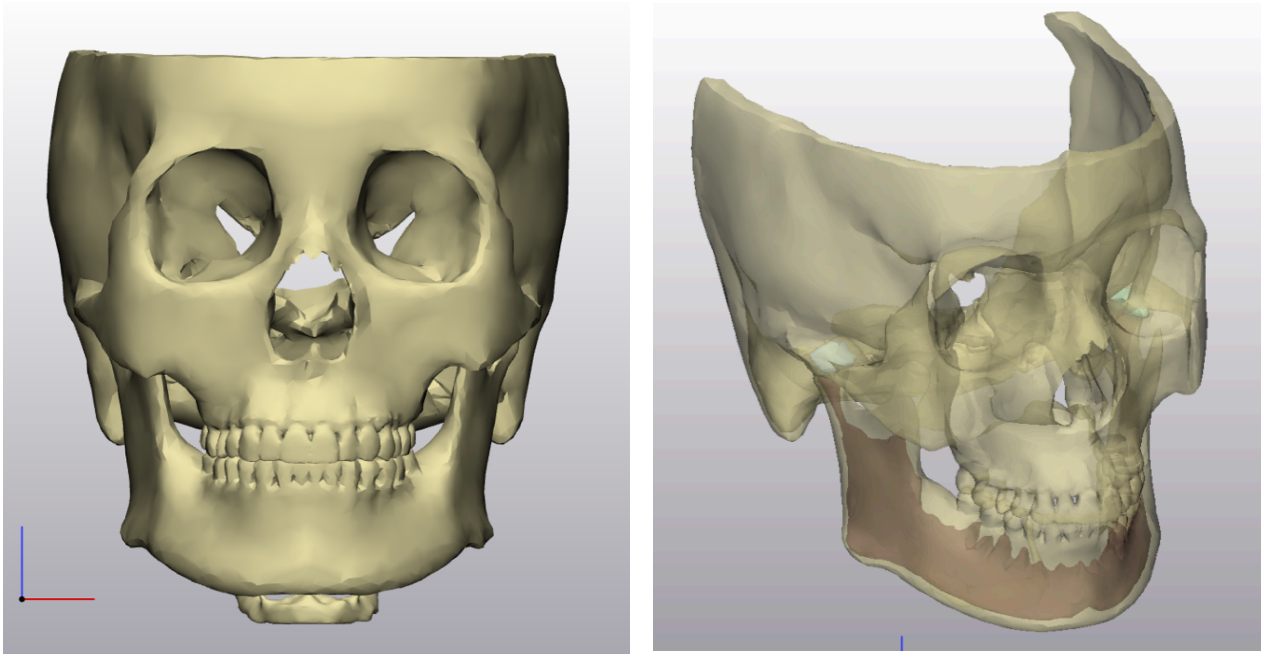

Figure 5: The whole skull. (a) Coronal view. (b) Transparent view. The mandibular cortical bone is hollow, and the cancellous bone totally matches the inside surface of the cortical bone.

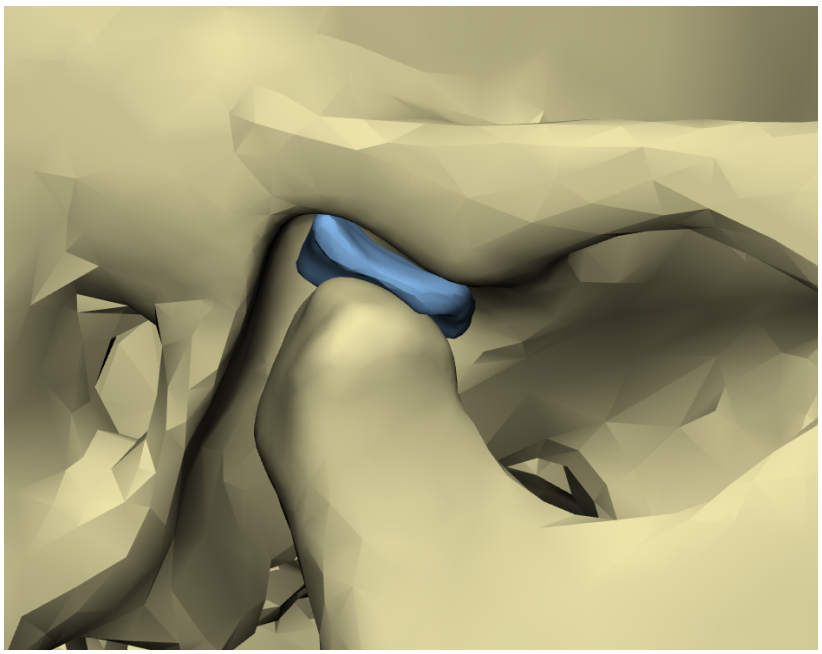

Figure 6: The prepared surface mesh of right TMJ in 3-Matic.

After the surface mesh of the model was prepared in 3-Matic, the finite element model was developed in MSC.Marc/Mentat 2020 for the simulation. First, the Abaqus files of surface meshes were imported into Marc/Mentat and checked. Then the glenoid fossa cartilage, condylar cartilage, retrodiscal lamina and discal ligament were created manually based on the anatomy (see Figures 7 and 8). At first, we did not use mesh to represent retrodiscal lamina and discal ligament; instead, we used springs/link elements as previously described by Koolstra and Sagl (Koolstra and van Eijden, 2005; Sagl et al., 2019). Springs/link elements however could not restrict the ACs properly, and the relatively free discs caused difficulty in convergence. Hence, we used volume mesh to represent them. After all the structures were volume meshed. Our model had a total of 37,111 nodes and 144,722 elements.

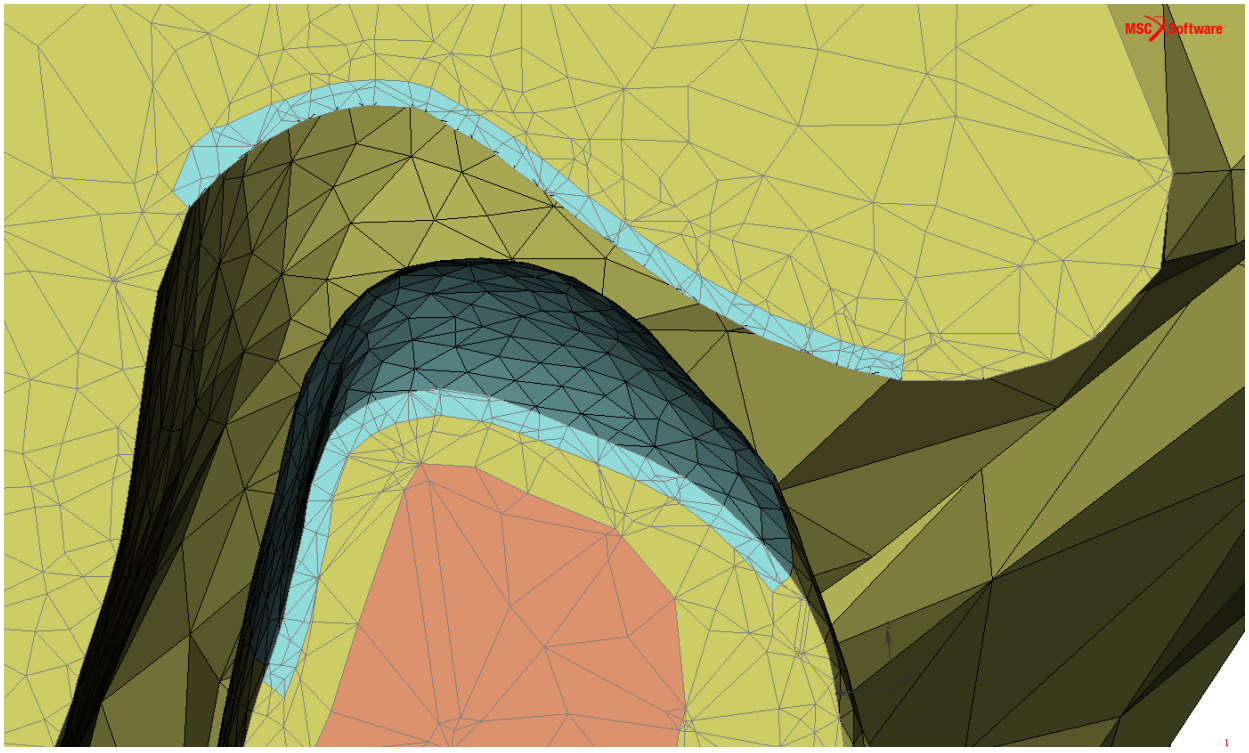

Figure 5: The sagital clipping view of the articular fossa and condyle of the right TMJ after volume meshing. The light blue elements represent cartilage with 0.4 mm thickness.

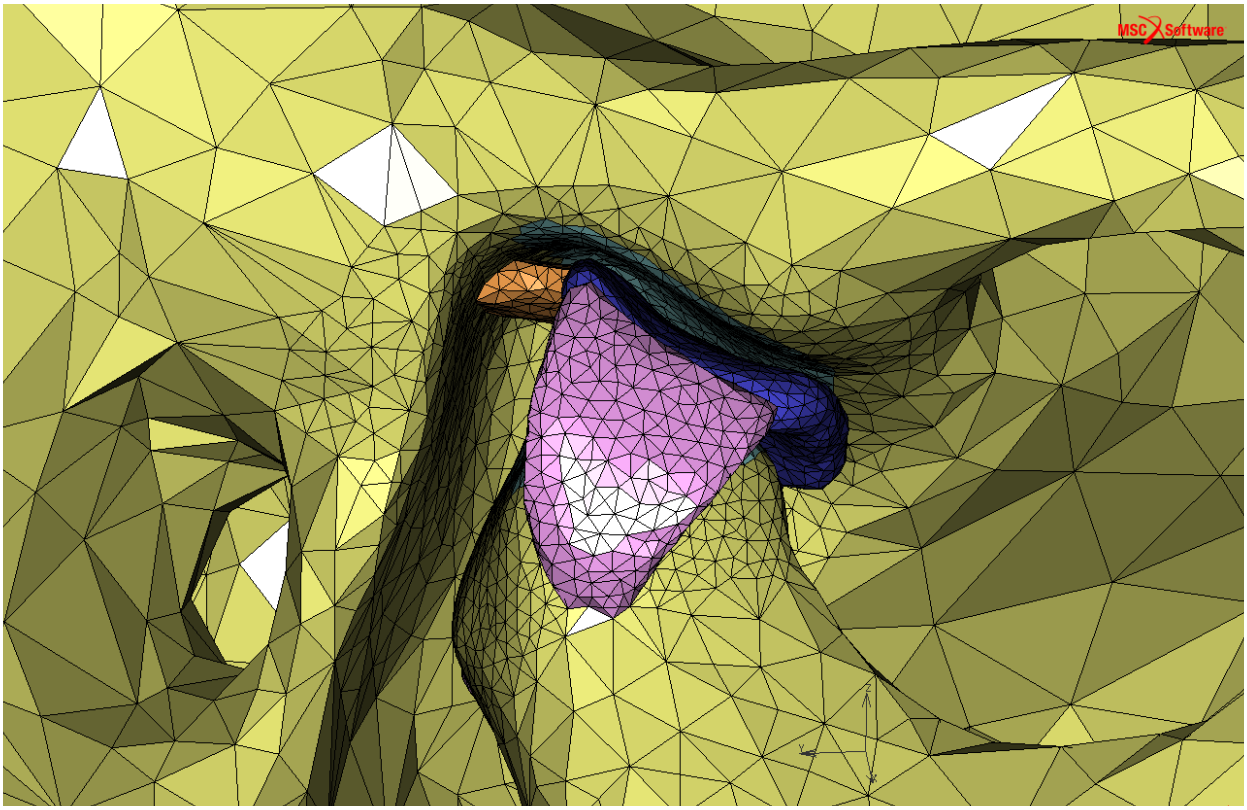

Figure 6: The sagital view of the right TMJ. The discal ligaments are in pink.

The skeletal structures, including cranium, maxilla, mandible, teeth and hyoid bone, were volume meshed into tetrahedral elements. The largely deformable tissues, namely cartilage, discs, discal ligaments and retrodiscal lamina, were meshed as hexahedral elements. Keilig investigated the performance of different classes of elements in an idealized bending test (Keilig, 2008). The deflection and load force maintained a linear relationship when the deflection was smaller than the thickness of the specimen, and the test could be simulated with the finite element method in this condition. The test was performed as 2-D simulations using linear and quadratic approaches for the triangle and quad elements with a variety of element sizes. As the result showed, the quad element yielded the most satisfactory results even with a relatively small number of elements. Furthermore, for the incompressible or nearly incompressible rubber-like material, the Herrmann formulation should be used to avoid a singularity caused by linear stress-strain law (Kumar, 2015; Hexagon, 2021). The number of elements, element class and type of each anatomical part are shown in Table 1.

Table 1: Number of elements, element class and type of each anatomical part.

Anatomical structures	Element Amount	Element Class	Element Type
Cranium	83,334	Tetrahedral	Tetra 134
Mandibular Cortical Bone	24,966	Tetrahedral	Tetra 134
Mandibular Cancellous Bone	5,417	Tetrahedral	Tetra 134
Left Disc	4,499	Hexahedral	Hex 84
Right Disc	4,429	Hexahedral	Hex 84
Left Glenoid Fossa Cartilage	2,047	Hexahedral	Hex 84
Right Glenoid Fossa Cartilage	2,209	Hexahedral	Hex 84
Left Condylar Cartilage	2,813	Hexahedral	Hex 84
Right Condylar Cartilage	2,450	Hexahedral	Hex 84
Left Discal Ligament	2,813	Hexahedral	Hex 84
Right Discal Ligament	3,850	Hexahedral	Hex 84
Left Retrodiscal Lamina	363	Hexahedral	Hex 84
Right Retrodiscal Lamina	606	Hexahedral	Hex 84
Hyoid Bone	5,578	Tetrahedral	Tetra 134

3.2 Completion of the finite element model

The finite element model was finalised in the following order: material properties were endowed, contact conditions were defined, and the biomechanical behaviour of masticatory muscles were represented.

3.2.1 Material properties

The physical property of an object is its natural character, which is essential for an FE simulation. Therefore, mechanical properties and density needed to be defined in our simulation. The skeletal structures and retrodiscal lamina were described as linear materials, their Young's modulus and Poisson's ratio shown in table 2 (Sun et al., 2015; Tanaka et al., 2007). As mentioned above, articular disc and cartilage have mainly hyperelastic, but also viscoelastic material characteristics. In order to simplify the material model for our study, we approximated the largely deformable tissues — the disc and the cartilage — according to the Mooney-Rivlin solid. This is the first hyperelastic material model developed by Ronald Rivlin and Melvin Moony (Mooney, 1940; Rivilin, 1947). For the incompressible rubber-like materials, the strain energy density function W is as shown in equation 1. C1 and C2 are constants that can be acquired from experiments, as shown in table 2 (Beek, et al., 2001; Beek, et al., 2003). I1 and I2 are the first and second invariants of the left Cauchy-Green deformation tensor B. Since there is insufficient experimental material data of the human TMJ ligament, its biomechanical behaviour is normally described like the medial collateral ligament of the knee. The TMJ ligament was approximated as Neo-Hookean solid, which is known as the one invariant version of Mooney-Rivlin, as equation 2 shows, and the constant is shown in table 2 (Commisso et al., 2014; Wan et al., 2011; Weiss and Gardiner, 2001).

$$W = C_1 (I_1\text{-}3) \qquad \textbf{Equation 1}$$

$$W = C_1 (I_1\text{-}3) + C_2 (I_2\text{-}3) \qquad \textbf{Equation 2}$$

3.2.2 Contact interactions

Contact phenomena happen widely in mechanical simulations. The contact interactions in the TMJ influence the movement of the condyles and the mandible. Therefore, it is very important to define the correct contact conditions. All the structures in the present study

were defined as deformable contact bodies, due to existing, predicted or potential contact interactions with surrounding tissues, with the exception of the hyoid bone and the mandibular cancellous bone.

The contacting interaction was specified in two contact tables: one for contacting bodies that have initial contact, the other one for contacting bodies that have contacting interaction during the simulations, as shown in table 3 and table 4. The interaction friction was 0.015 (Commisso et al., 2018).

Since we used linear finite elements with a faceted description, in default the shape of the contact body describes the interacting boundary. The normal of the body is not always continuous for a curved boundary, which can lead to poor precision. Therefore, the contacting bodies were smoothed by replacing the finite segment with an analytical entity of a coons surface. Consequently, the nodes of a contacting body will touch it instead of the actual finite elements. Moreover, the coons surface will update as the finite element body deforms.

Table 2: Material properties of the parts.

Material	Linear Material		Hyperelastic Material		Mass Density (kg/m^3)
	Young's modulus (MPa)	Poisson's ratio	Constant C1 (MPa)	Constant C2 (MPa)	
Cortical bone	13700.0	0.30			1740
Cancellous bone	7930	0.30			8700
Retrodiscal laminare	1.5	0.4			1170
Disc			9×10^{-1}	9×10^{-4}	1233
Cartilage			4.5×10^{-1}	4.5×10^{-4}	1100
Discal ligament			6.43		1170

Table 3: Initial contact table. Cranium and mandible have initial contact at dental area before the simulation, and the contact relation is touch.

Body name	Cranium
Mandibular Cortical Bone	contact relation: touch

Table 4: Contact table of the whole model. The contact pairs that might touch each other during the simulation are marked with T. The contact bodies are: 1. Cranium 2. Left disc 3. Left condylar cartilage 4. Left glenoid fossa cartilage 5. Right disc 6. Right condylar cartilage 7. Right glenoid fossa cartilage 8. Mandible 9. Left discal ligament 10. Right discal ligament 11. Left retrodiscal lamina 12. Right retrodiscal lamina.

Body number	1	2	3	4	5	6	7	8	9	10	11	12
1		T			T			T	T	T		
2	T		T	T								
3		T		T					T			
4		T	T						T		T	
5	T					T	T					
6					T		T			T		
7					T	T				T		T
8	T											
9	T		T	T								
10	T					T	T					
11				T								
12							T					

3.2.3 Generation of masticatory muscle systems

The masticatory muscle system was represented based on Hill's type muscle model. The larger muscles were split into several groups according to literature to accurately reproduce the biomechanical muscle behaviours (van Eijden et al., 1997). Each group of muscle was simplified into point-to-point muscle as shown in Figure 9. Altogether, the mandible was activated by 12 pairs of muscles with architectural parameters as shown in Table 5.

Table 5: The architectural parameters of muscles.

Muscles	Muscle length (mm)	Max. force (N)	CE length (mm)	SE length (mm)
Superficial masseter	50.0	272.8	30.0	25.0
Deep masseter	30.8	139.6	24.6	23.1
Anterior temporalis	60.4	105.0	33.9	30.2
Middle temporalis	64.5	85.8	37.4	32.3
Posterior temporalis	73.5	74.2	37.8	36.7
Medial pterygoid	42.0	240.0	30.0	28.0
Superior lateral pterygoid	29.0	38.0	21.5	9.4
Inferior lateral pterygoid	37.8	112.8	20.3	9.0
Anterior belly of digastric	43.0	46.4	42.6	3.0
Geniohyoid	40.7	38.8	35.3	5.4
Anterior mylohyoid	32.7	63.6	24.0	0.0
Posterior mylohyoid	37.7	21.2	39.7	0.0

The active muscle forces were applied as one-dimensional force vectors. Firstly, a local coordinate system was defined to build a specific coordinate for each group of muscles, to apply the forces along with the orientation of the muscles. We used a rectangular coordinate system, specified by three nodes called node A, B and C. Node A is the origin of the local coordinate system, which was set as the anatomical insertion of elevator muscles and lateral pterygoid, as well as the anatomical origin of the depressor muscles. Node B indicates the z-axis, which was set as the anatomical origin of elevators and lateral pterygoid, and the anatomical insertion of depressors. Thus, the z-axis represented the orientation of muscles, and node A was the loading node on the mandible. Node A was created with 1 mm distance from the loading surface, then connected by 6DOF links with nodes on the loading area. Therefore, the force would be distributed averagely through the links. Node C indicated the x-axis and was defined as a random node excluding nodes A and B. Node C is relatively irrelevant, only to form the local coordinate system.

Since the position of node A in the global coordinate would change as the mandible displaced during the simulation, the location of node A needed to be updated through a transforming function. In this way, the active muscle force was always applied along with the origin and insertion of the muscles. As MSC.Marc/Mentat does not support a method to define the velocity-force relation and the distance-force relation of the active muscle force, the force was restricted by the time-force function with the help of the simulation result from literature as shown in Figure 10 (Koolstra and van Eijden, 2006).

The passive muscle forces were simulated as springs. Since the passive muscle forces of mouth depressors are negligible, the springs were only applied for the elevator muscles. The springs were defined with the same nodes as in the local coordinate node A and B for each muscle and with a freedom of the spring along the spring direction. The biomechanical behaviour was described as the equation 3 (Martins et al., 1997).

$$Fp = \begin{cases} F_0 \times 4(L_m/L_0 - 1)^2, & for\ L_m > L_0 \\ 0, & otherweise \end{cases}$$ **Equation 3**

F_p: passive muscle force;
F_0: the maximum muscle force;
L_0: the optimal muscle length;
L_m: the stretched muscle length.

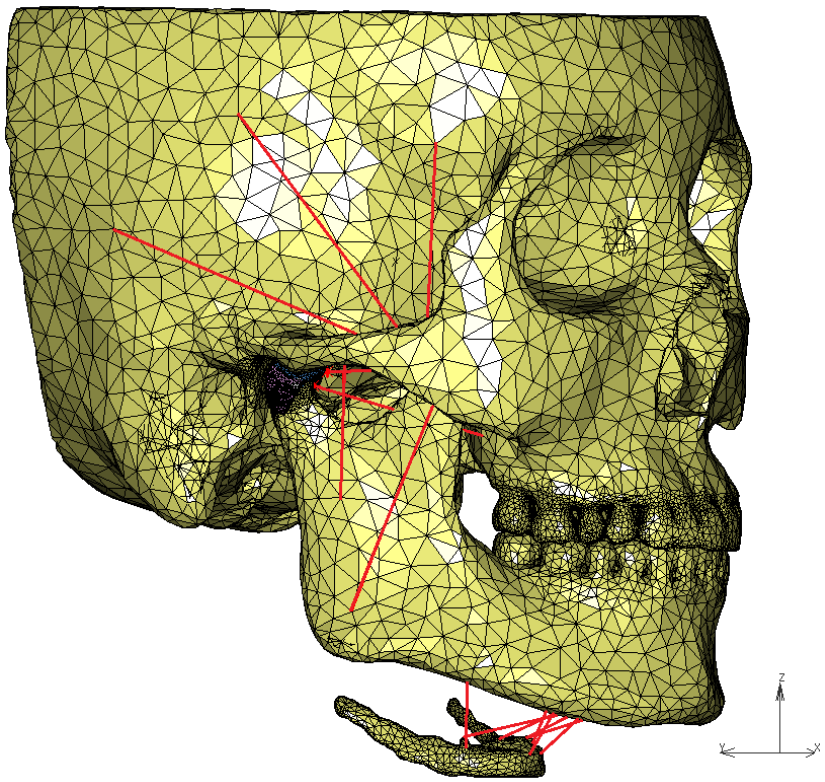

Figure 8: The red lines represent the direction the Hill type point-to-point muscles. The larger muscles were split up into several muscle groups according to literature (van Eijden et al., 1997).

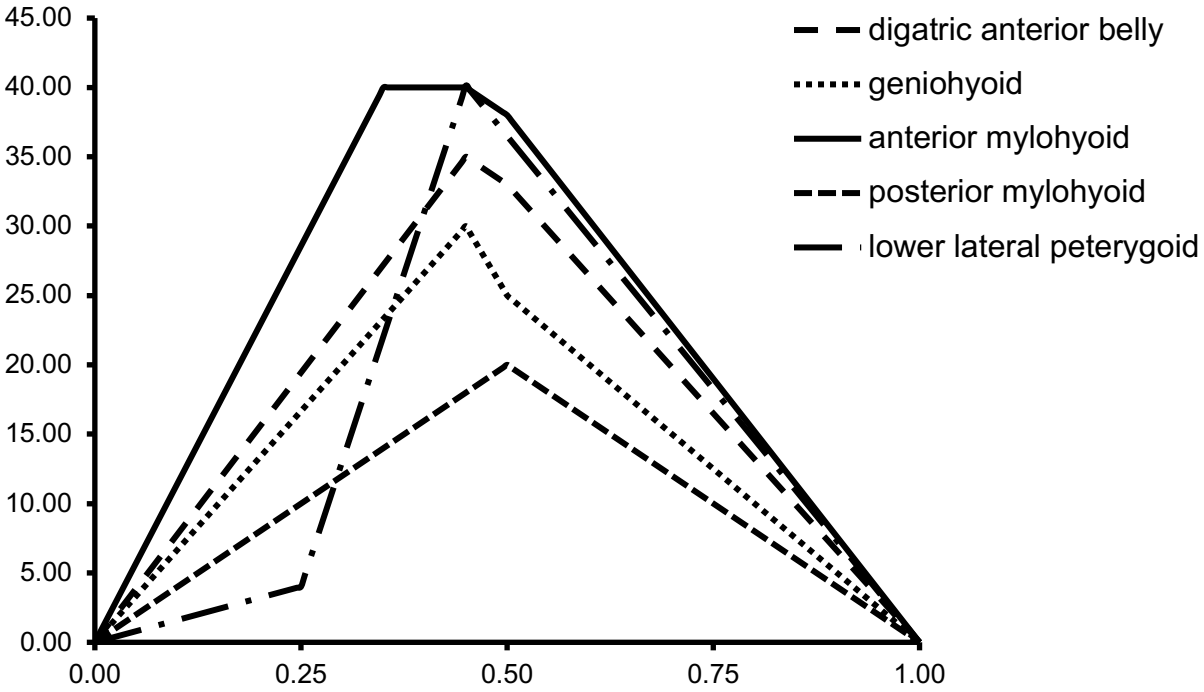

Figure 7: force-time relation of the active force of depressors.

3.2.4 Boundary conditions

To simulate the mouth opening without a head backward rotation and the translation of the hyoid bone, the cranium and hyoid bone were fixed on the border as shown in Figure 11. The fixed displacement was applied on 1185 nodes in 3 dimensions with a value of 0 mm.

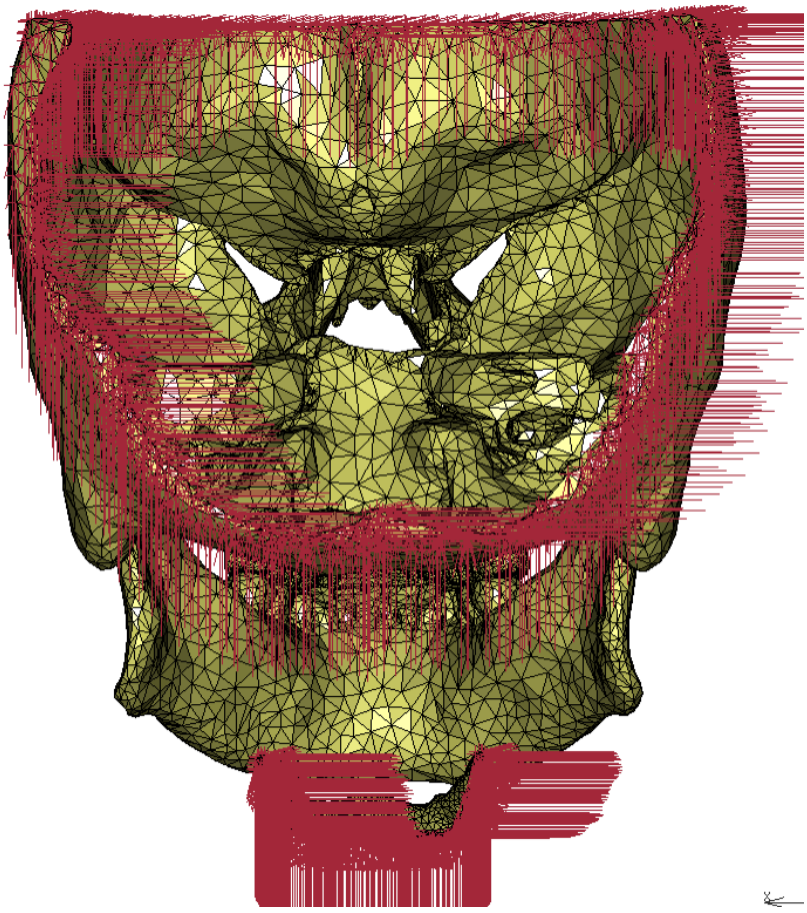

Figure 9: the cranium and hyoid bone were fixed on the border with boundary.

3.3 Preparation of models with different configurations of OEs

Until now, we built our first model, which was a reference model named as Model WOOE. Then another seven models were developed based on Model WOOE, each of them with a configuration of OEs. The only difference among them was without or with variations of OEs. The models and their OEs are shown in Table 6. The elastics were represented with springs, and their mechanical behaviours were referred to the product information of “Latex Elastics” from the company “American Orthodontics”. The primary elastic force was set as “medium force” –around 1.25 N.

Table 6: Models and their corresponding OEs. The located teeth of the OEs were described through the international tooth numbering system.

Model	Name of OE	Configuration
WOOE	Without OE	No configuration
CII	Class II	Right: between 12 and 13 to 46 Left: between 22 and 23 to 36
CIII	Class III	Right: between 42 and 43 to 16 Left: between 32 and 33 to 26
CIIs	Class II short	Right: 13 to 44 and 45 Left: 23 to 34 and 35
CIIIs	Class III short	Right: 43 to 14 and 15 Left: 33 to 24 and 25
ATT	Anterior teeth traction	12 to 33
MT	Molar traction	17 to 47
VT	Vertical traction	Right: 13 to 43 and 44 Left: 23 to 33 and 34

3.4 Simulation

Mouth opening, closing and clenching were simulated in Model WOOE to verify the model. The total load time of mouth opening and closing was 1 s with a constant time step of 0.005 s. The mouth depressors and elevators were fully activated in this task. At first we tried larger time steps, this however caused the simulation to stop in a very early stage. The model could not withstand too much force in one step. For clenching, the elevators were isometrically activated 1 % and 10 % separately with a load time of 0.1 s, and the constant time step of clenching was 0.001 s. Mouth opening and closing were also simulated in the other models to investigate the effect of OEs on TMJ. The data of Maximum principal stress (MaxPS) in the disc and condylar cartilage and the displacement of the mandible were collected. The mandibular displacement was analysed through five nodes

which corresponded to cephalometric landmarks (see Figure 12): condylion (Co, on the bilateral condyles), gonion (Go, on the tip of bilateral mandibular angels), and gnathion (Gn, on the chin) (Vallabh et al., 2020).

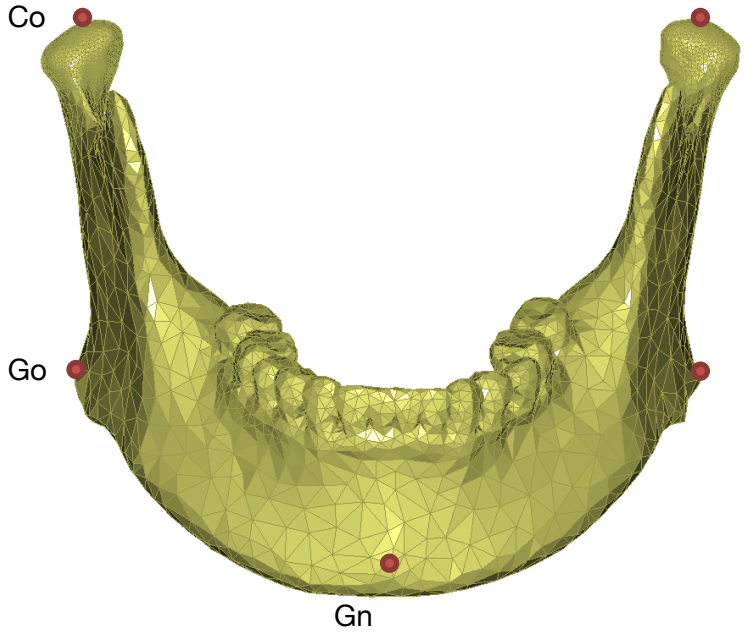

Figure 10: the five nodes on mandible corresponding to cephalometric landmarks: condylion (Co), gonion (Go) and gnathion (Gn).

4. Results

The results were displayed in the postprocessor of MSC.Marc/Mentat 2020, which visually well displayed the displacements of different structures and distribution and magnitude of stresses. The colour maps of results shown by vectors and contour band indicated the magnitude and direction of the scalars, from blue (the minimum) to red (the maximum). In addition, out of range results were illustrated in light grey (larger than the maximum) or dark grey (lower than the minimum).

4.1 Reference model

Figures 13-18 show the results of the reference model, WOOE (without OEs). Figures 13 and 14 show the results of mouth opening at 0.25 s and 0.45 s in coronal view and sagittal view in vectors. The displacement of the mandible, according to the vectors, was symmetrical. By inspecting the results step by step, the mandible was mainly rotating with the condyles as rotation centres, until the inter-incisal gap was around 25.0 mm. After 0.25 s, the condyles began to slide forward and downwards along the posterior slope of the maxillary articular eminence, while the whole mandible was still rotating. The maximum mouth opening was reached at 0.45 s with the largest inter-incisal gap of 30.0 mm as shown in Figure 14. After 0.45 s, the mouth began to close with the mandible rotating counterclockwise, while the condyles slid backward to the glenoid fossa.

Figure 15 shows the displacement of the five reference nodes in three dimensions. Figure 15 (a) shows the displacement on the x-axis in which the five nodes had slight horizontal movement. During mouth opening, except for the positive movement of Gn, which was towards the left side of the model, the trend of the other four nodes was negative towards the right side. Between 0.25-0.29 s, Gn had a sharp drop from 0.6 mm to 0.3 mm, after that, the Gn continually increased to 0.9 mm until 0.53 s, then it decreased to zero. The left Co had a relative sharper dive after 0.25 s, which was -0.1 mm to -0.9 mm. Compared with the left Co, the right Co and both Gos decreased gradually to the lowest point, which was -0.5, -0.3 and -0.2 mm respectively, then increased to 0 mm.

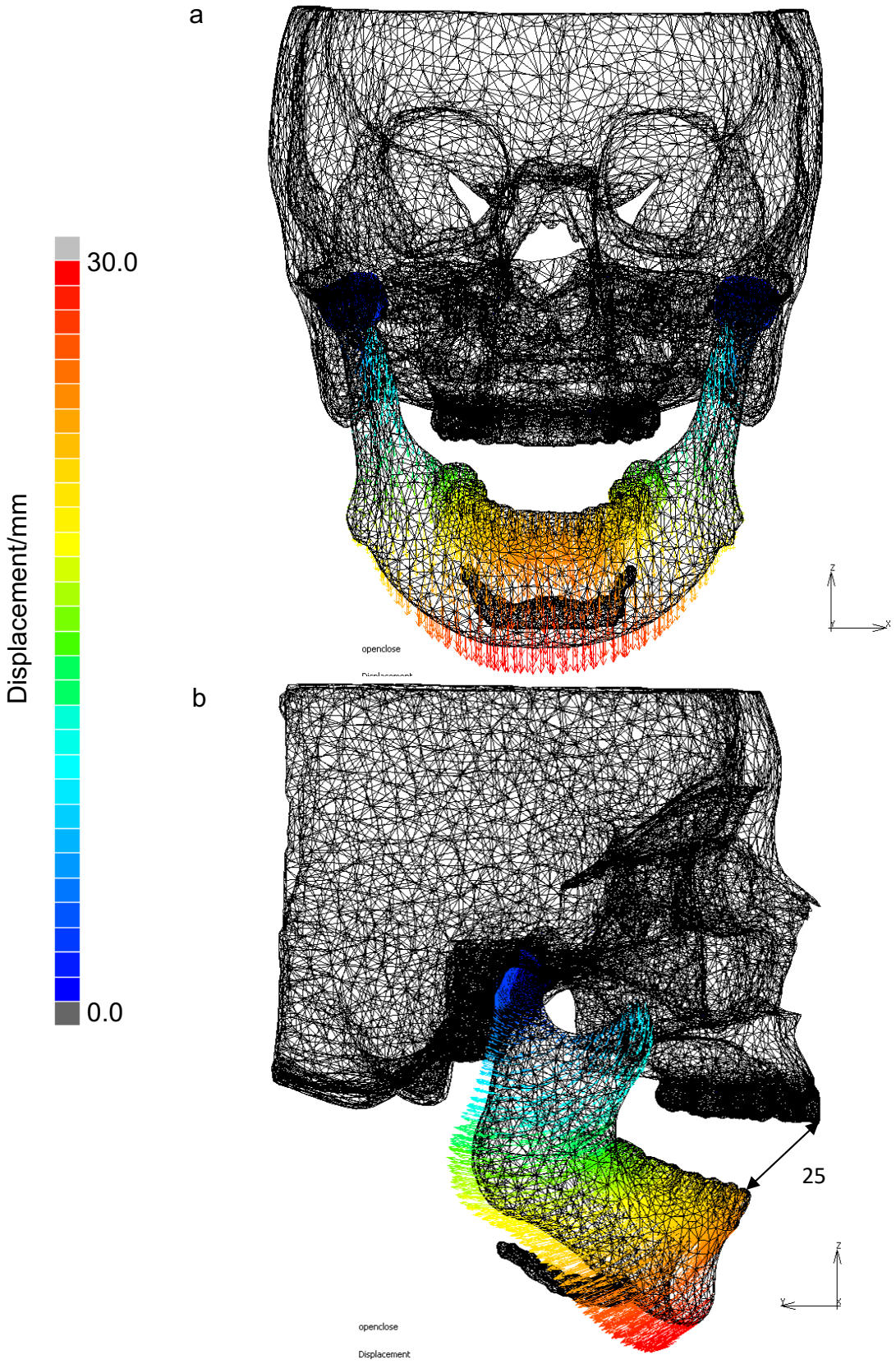

Figure 11: Displacement of the mandible at 0.25 s, the inner-incisor gap reached 25.0 mm.

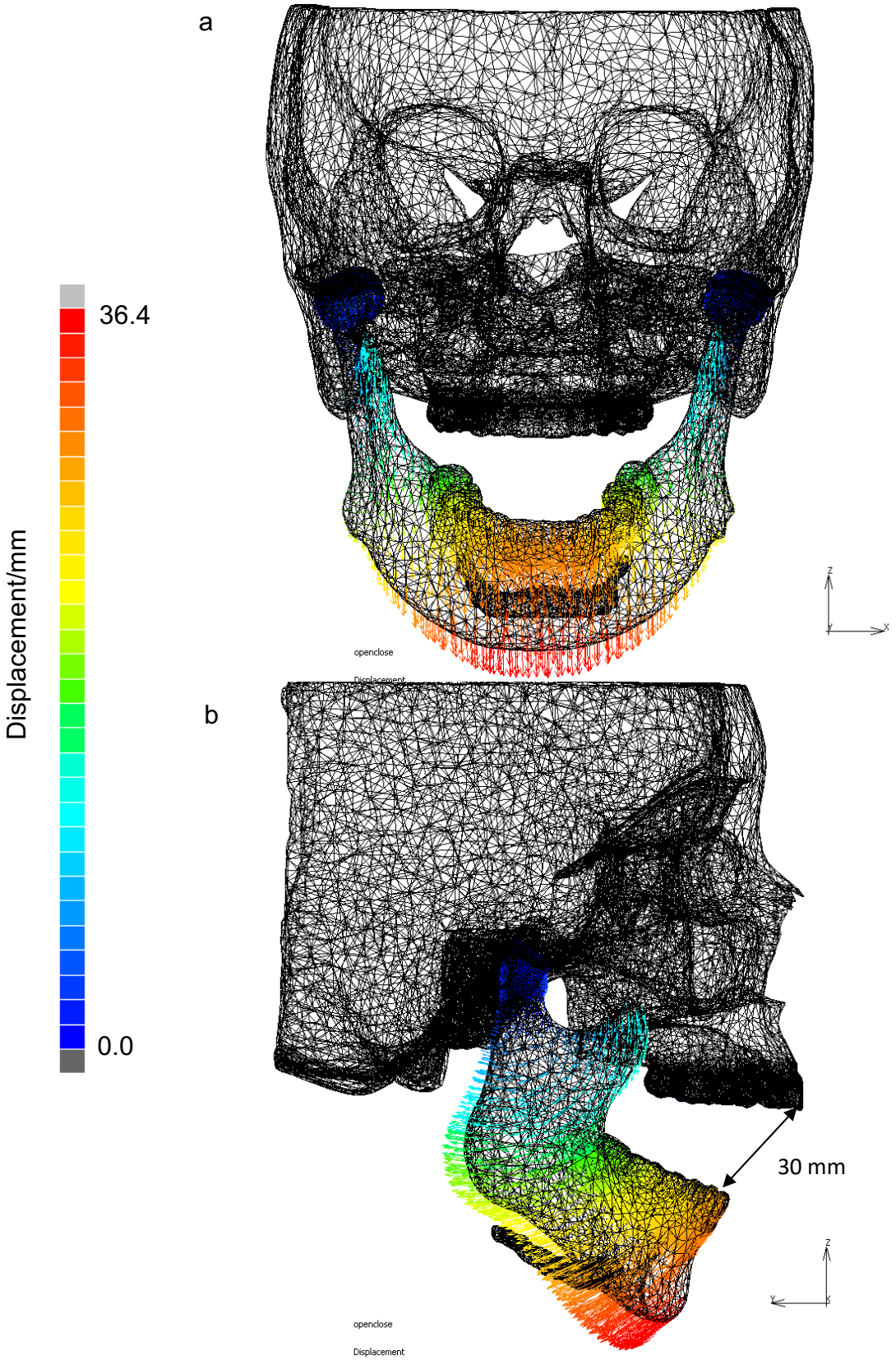

Figure 12: Displacement of the mandible at 0.45 s, the inner-incisor gap reached 30.0 mm.

Figure 15 (b) shows the displacement of the five reference nodes on the y-axis. Gn left and right Gos demonstrated a positive nonlinear movement before 0.45 s, which increased dramatically before 0.2 s. Afterwards, the rising trend became relatively flat to 29.3, 19.6 and 18.1 mm respectively. At 0.45 s, the curves showed a flat decrease then followed by a rapid decline to 0 mm. The left and right Co remained on the negative side of the y-axis during the whole mouth open-close simulation. Before 0.25 s, the two Cos had barely no displacement, but after 0.25 s, they declined moderately to the lower point, which was -2.9 and -4.5 mm, then gradually climbed back to 0 mm. Thus, according to the moving trend of the five reference nodes, the mandibular body moved backward before 0.45 s, then moved forward to the start point at the end of the simulation. While the condyles stayed in place before 0.25 s, then moved forward before 0.5 s, afterwards translated back to the start point.

Figure 15 (c) illustrates the displacement of the reference nodes on the z-axis. Except for Gn, the other four nodes were all on the positive side. Gn had a dramatic decline from 0 to 0.2 s then the decline became moderate to a low point of -21.5 mm at 0.45 s them increased to -0.4 mm at the end of the simulation. The left and right Co increased from 0 to 0.17 s then was maintained at about 0.08 s. From 0.25 s, declination started from 1.8 to 0.9 mm and from 1.5 to 0 mm respectively. The left Go rose from the start until 0.25s reaching the point of 1.8 mm, then it had an oscillating climbing movement until 0.45 s. Subsequently it decreased until the end of the simulation whereas the right Go rose from the start until 0.28 s reaching 2.3 mm, then it declined to 0 mm.

Figure 16 shows the stress distribution in the discs. On the left disc (a), the highest compressive stress was in the middle of the intermediate zone, which was -28.2 MPa, and the highest tensile stresses (33.8 MPa) were on the anterior side of the anterior band. According to the distribution of the colours, stresses on the major area of the disc were between -5.0 to 5.0 MPa. Relative higher stresses with a magnitude around 10.0 (compressive (light blue) and tensile (yellow)) were scattered over the whole surface of the disc. On the right disc (b), the highest compressive stresses (-38.0) were also in the intermediate zone but more anterior and medial, while the highest tensile stresses (29.2) were on the lateral side of the disc.

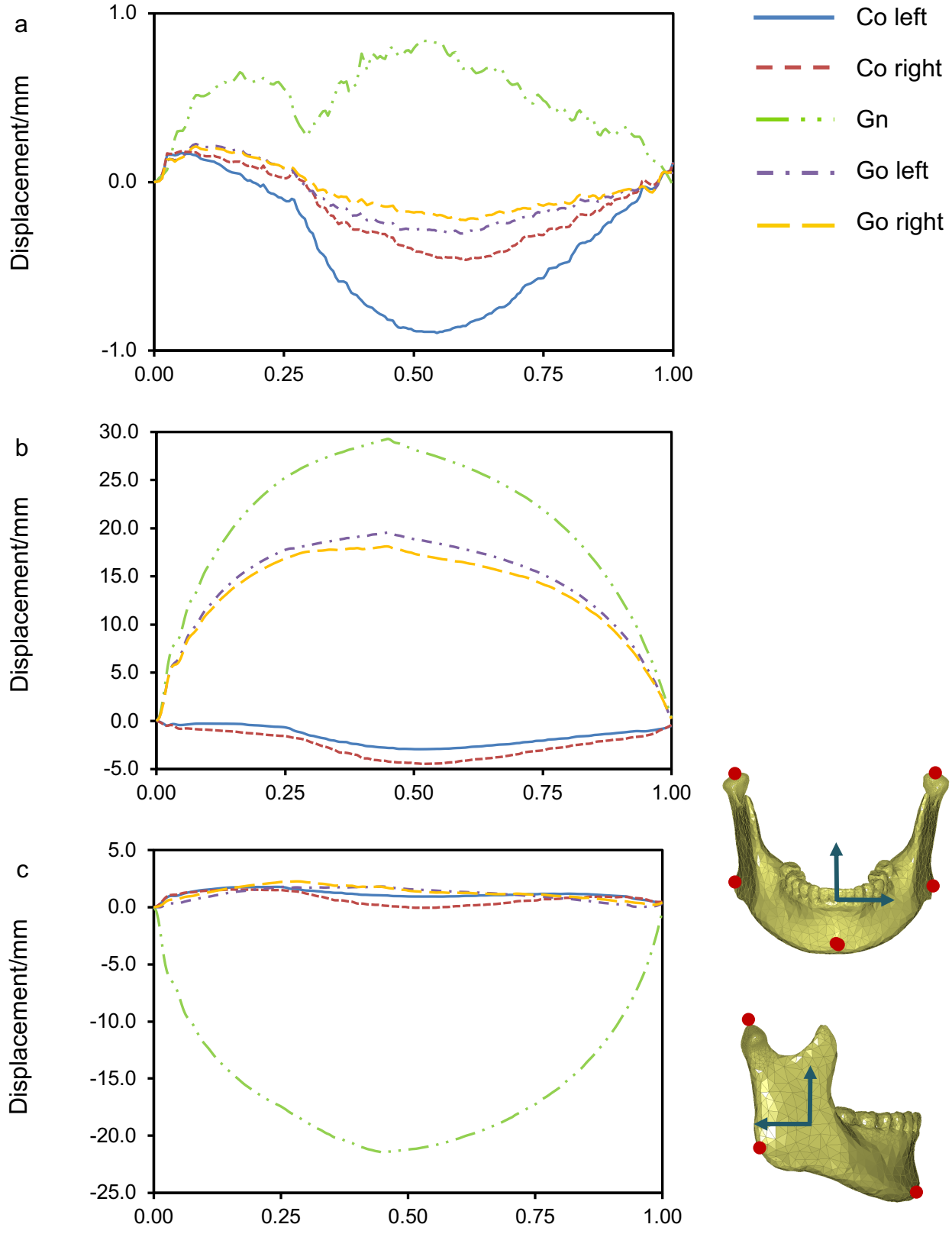

Figure 13: Displacement of the five reference nodes in three dimensions. (a) X-axis (b) Y-axis (c) Z-axis.

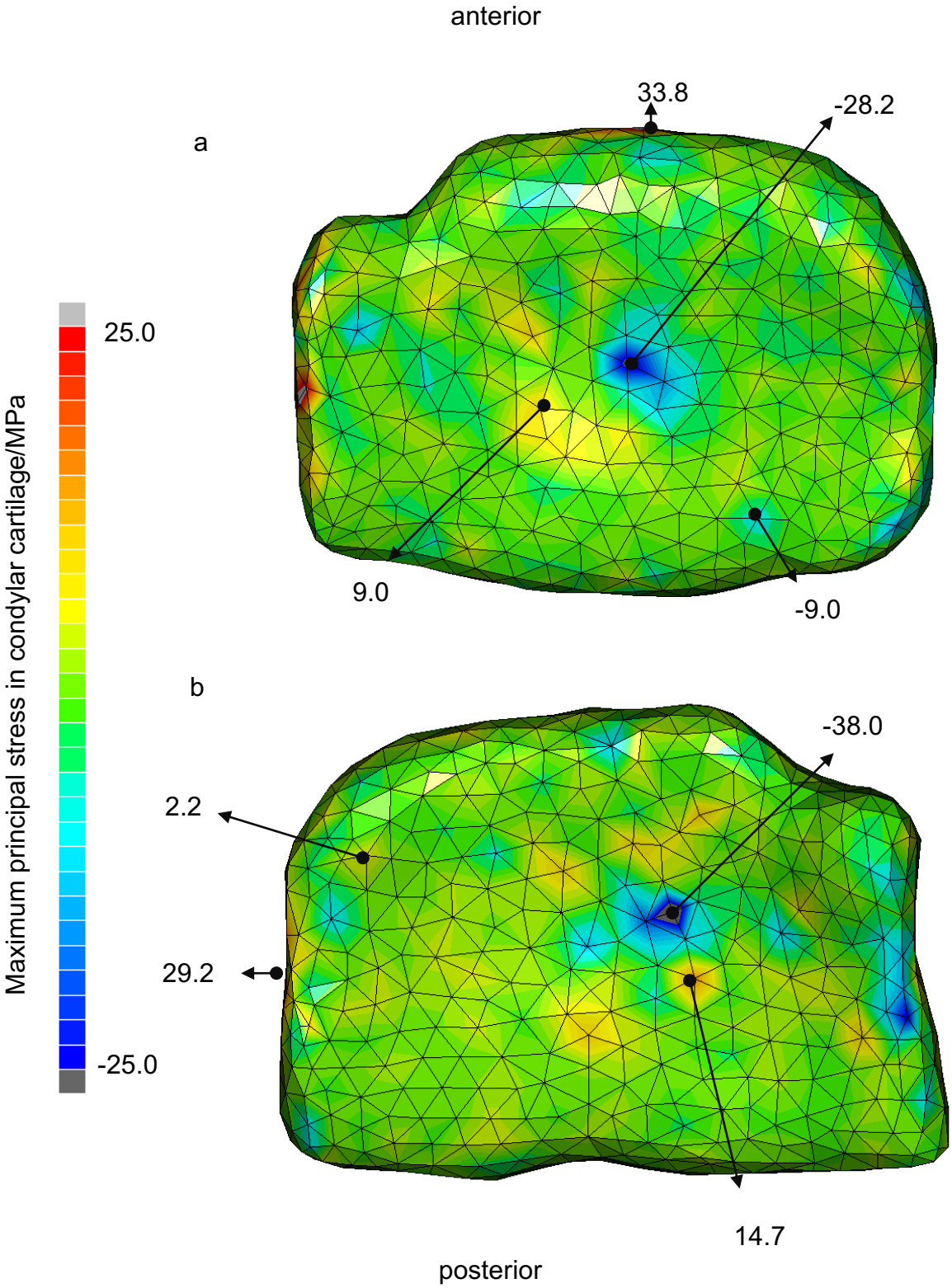

Figure 14: The Maximum principal stress on the surface of articular side of the left (a) and right (b) TMJ discs.

Figures 17 and 18 show the stress distribution in the left and condylar cartilage, on the articular side and the condylar side. The maximum principal stress (MaxPS) in the majority area of the cartilage was between -1 and 1 MPa. The lowest compressive stresses were on the anterior slope and the condylar side of the left and right condylar cartilages, which were -30.4 and -38.3 MPa respectively. The highest tensile stresses of the two condylar cartilages were both on the condylar crest and the condylar side of the cartilages with a value of 3.0 MPa.

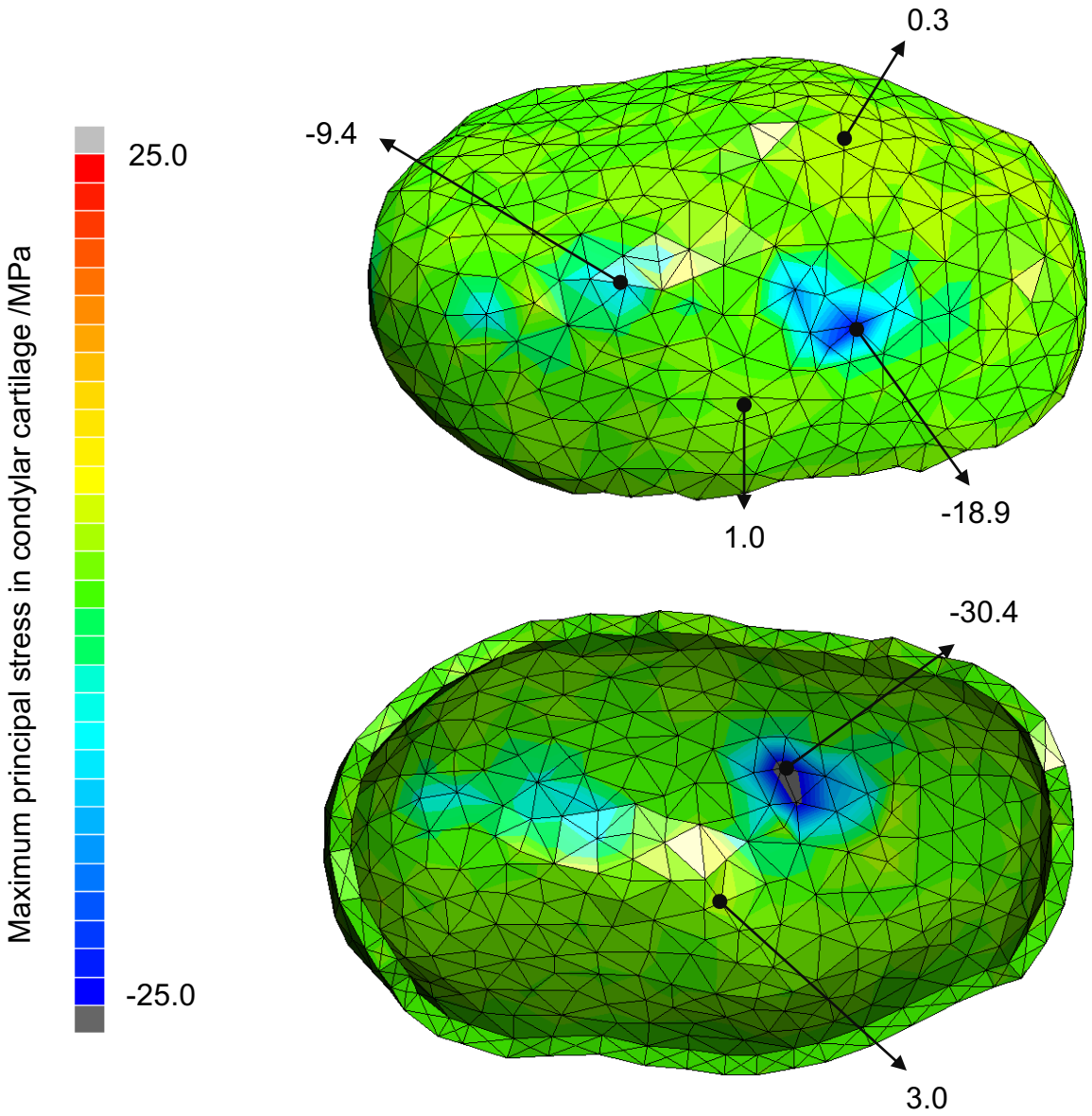

Figure 15: Maximum principal stress on the left articular cartilage, articular side (upper) and condylar side (lower).

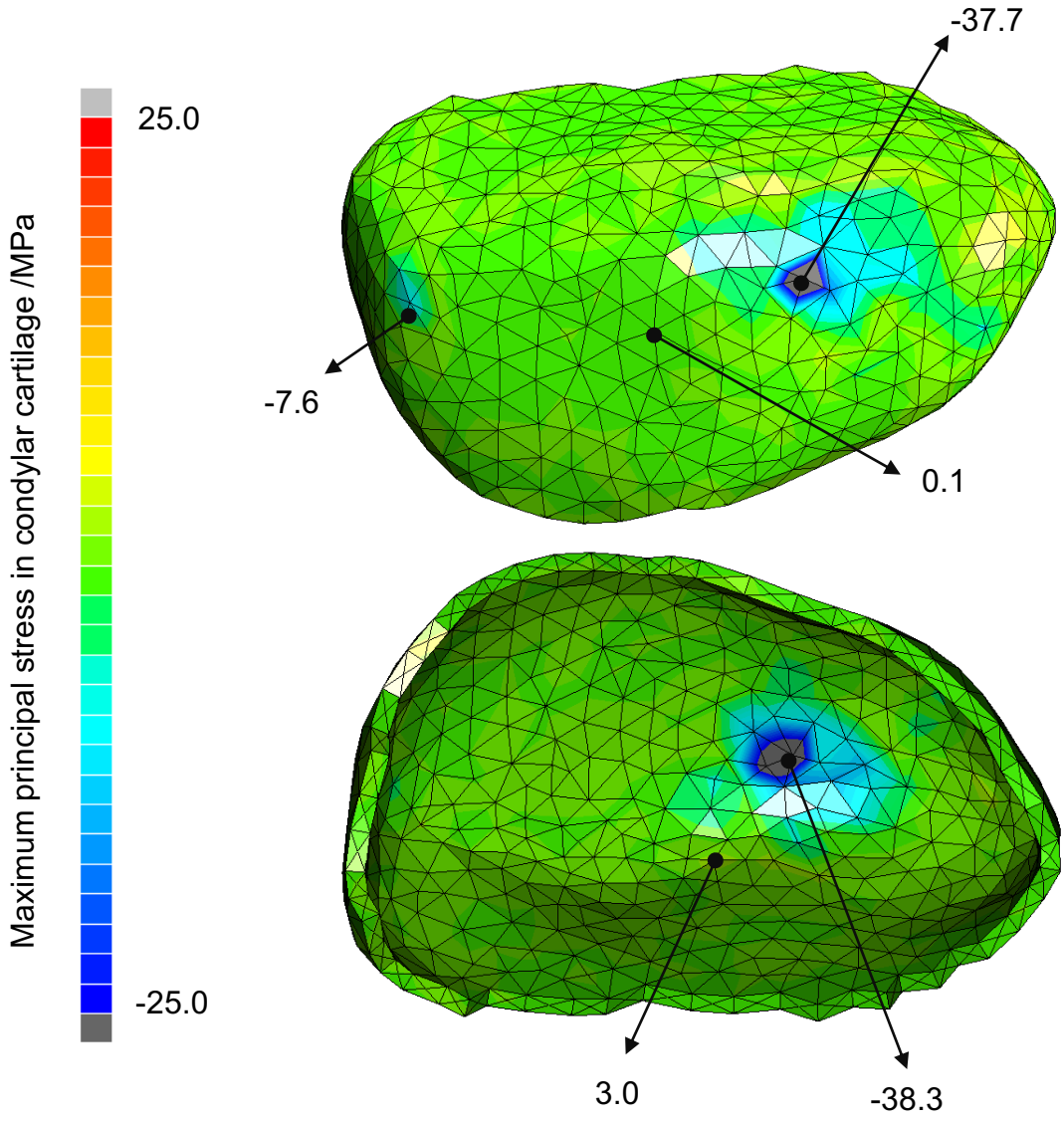

Figure 16: Maximum principal stress on the right articular cartilage, articular side (upper) and condylar side (lower).

4.2 Comparison of the results of the variants

Figures 19-23 show the time-displacement graphs of the five reference nodes in eight models. Overall results showed highly similar patterns and magnitudes of movements in three dimensions. The only exceptions were observed in the displacement of Model ATT and MT on the x-axis, with anterior teeth traction and molar traction respectively. The displacement on the x-axis of all five reference nodes of Model ATT and MT showed an obvious negative displacement in the very early stage of mouth opening. This phenomenon was corrected after 0.06 s in Model ATT and 0.055 s in Model MT. After 0.15 s, both

condylions showed no significant difference in the movement on the x-axis. While the curves of gnathion and gonion, with unsymmetrical elastics, were still in a relatively lower position in the graphic compared with the curves without elastics or with symmetrical elastics.

The largest difference of the displacement on the x-axis between Model WOOE and Model ATT was observed at 0.02 s. For ATT Model, the difference was -0.37 mm on the left Co (WOOE was 0.09 mm), -0.35 mm on the right Co (Model WOOE was 0.10 mm), -1.27 mm on the Gn (Model WOOE was 0.05 mm), -0.57 mm on the left Go (Model WOOE was 0.08 mm), and -0.54 mm on the right Go (Model WOOE was 0.08 mm). Moreover, the biggest displacement difference on the x-axis between Model WOOE and Model MT happened at 0.015s. -0.25 mm was recorded for Model MT on the left and right Co (Model WOOE was 0.04 mm on both Cos), -0.45 mm on Gn (Model WOOE was 0.04 mm), and -0.39 mm on the left and right Go (Model WOOE was 0.02 mm on both Gos).

Although there was no great difference in the displacement on the y- and z-axis among the models, still some different trends between Model WOOE and the others could be identified. Before 0.02 s, the displacement on the y-axis of the left and right Co of Model CIII, CIIIs, VT and the right Co of Model ATT increased to the top point while the other models decreased. This means that the condyles of Models CIII, CIIIs and VT were moving backward, while the condyles of the other models were moving forward. However, the Model ATT was different, in which the left condyle was moving forward, while the right condyle was moving backward. After 0.02 s and before 0.25 s, the curves of the left and right Cos of Models CIII, CIIIs and VT were above the curves of the other models, which means that the condyles were relatively more backward.

The displacements of Model CIII, CIIIs and VT on the z-axis before 0.25 s had a similar pattern. With the combination of the displacement on the y- and z-axis of the five reference nodes, the sagittal kinetic behaviour of the mandible could be determined. Both Cos and Gos of Model CII moved more forward and downward, and Gn moved more forward compared with Model WOOE, which means that Model II had a clockwise kinetic trend. Although both Cos of Model CIII and CIIIs moved more backward and upward compared to Model WOOE, the Gos moved more upward, which means that Model CIII and CIIIs had a counter-clockwise kinetic trend.

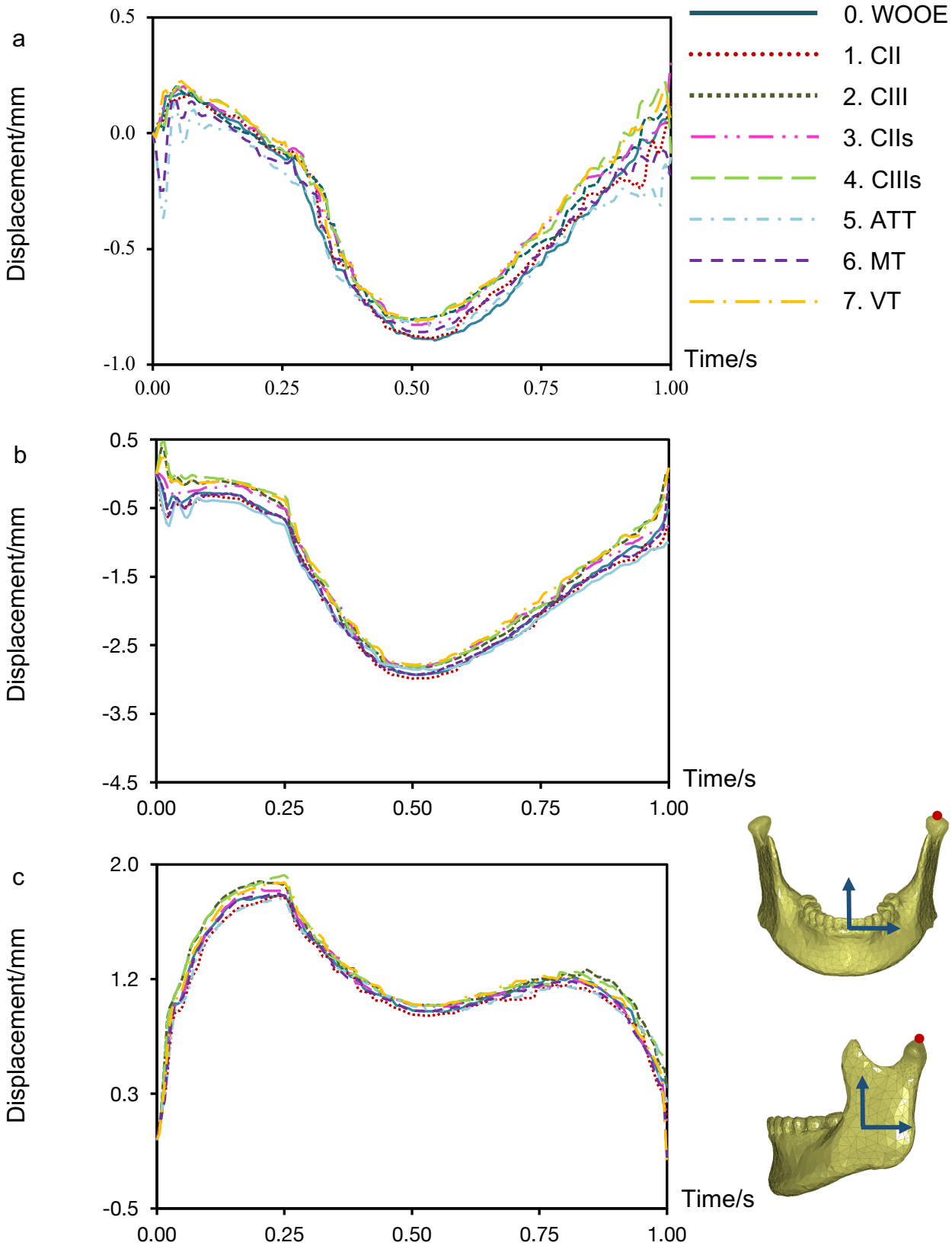

Figure 17: Displacement of reference node left Co of the 8 models. (a) X-axis (b) Y-axis (c) Z-axis.

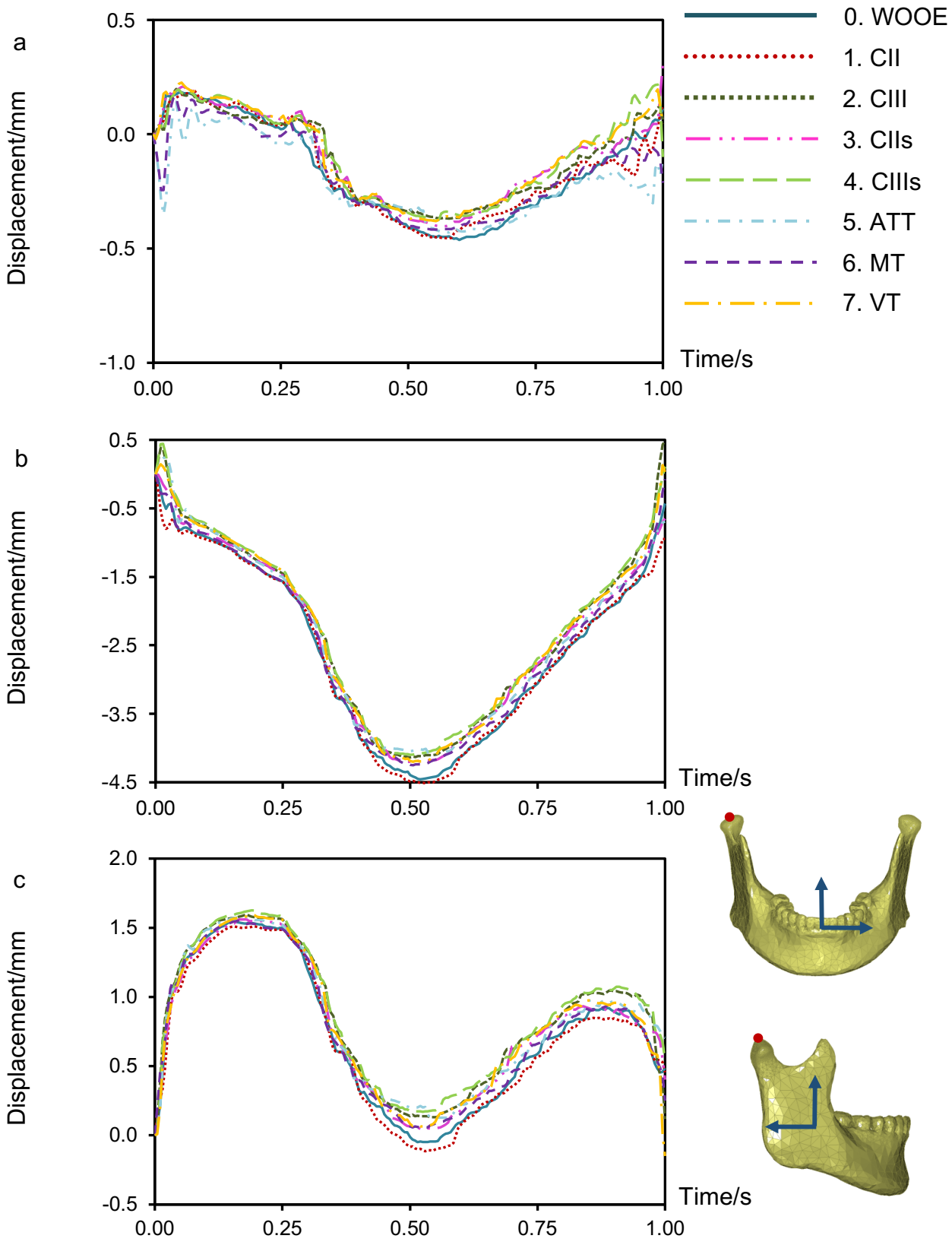

Figure 18: Displacement of the reference node right Co of the 8 models. (a) X-axis (b) Y-axis (c) Z-axis.

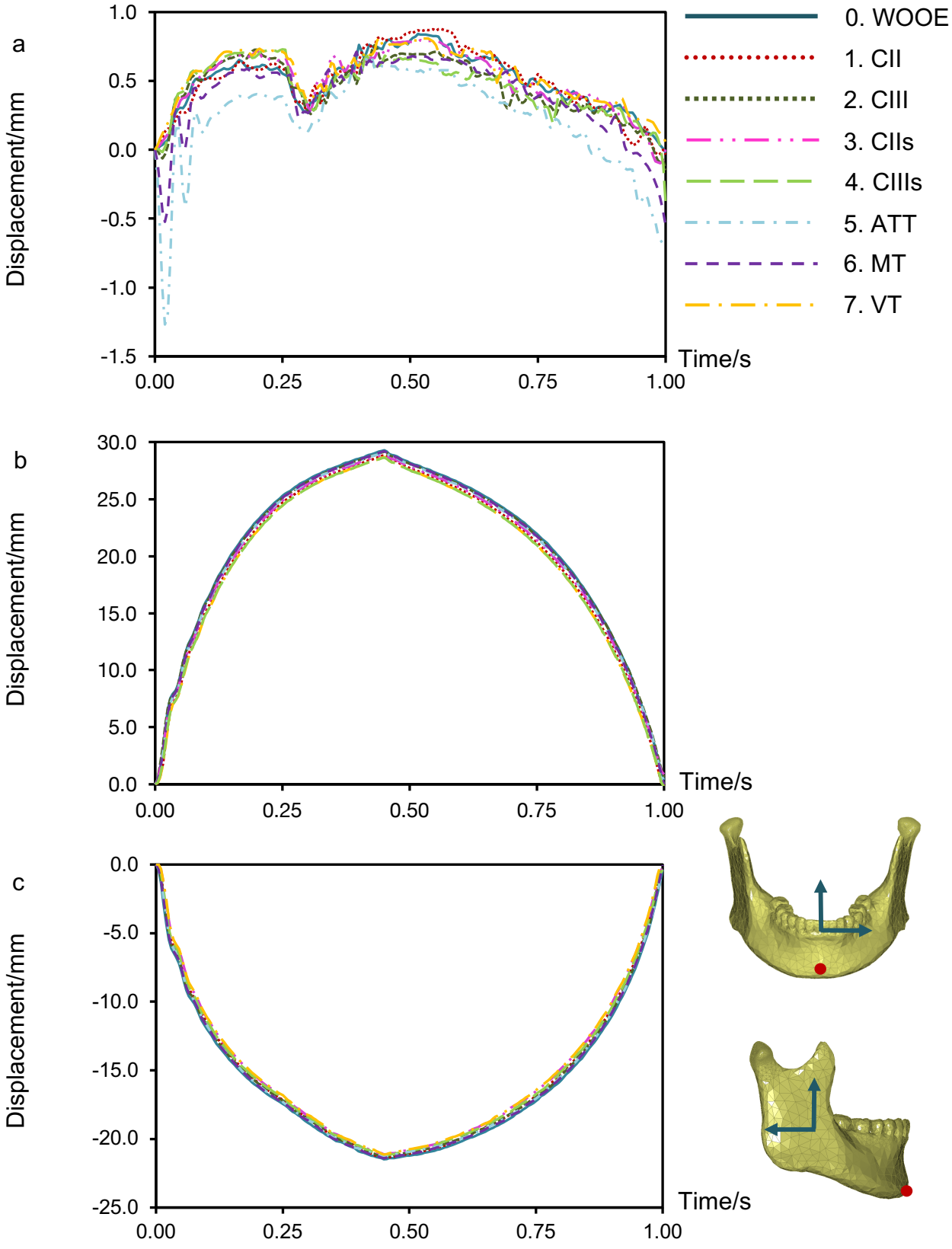

Figure 19: Displacement of the reference node Gn of the 8 models. (a) X-axis (b) Y-axis (c) Z-axis.

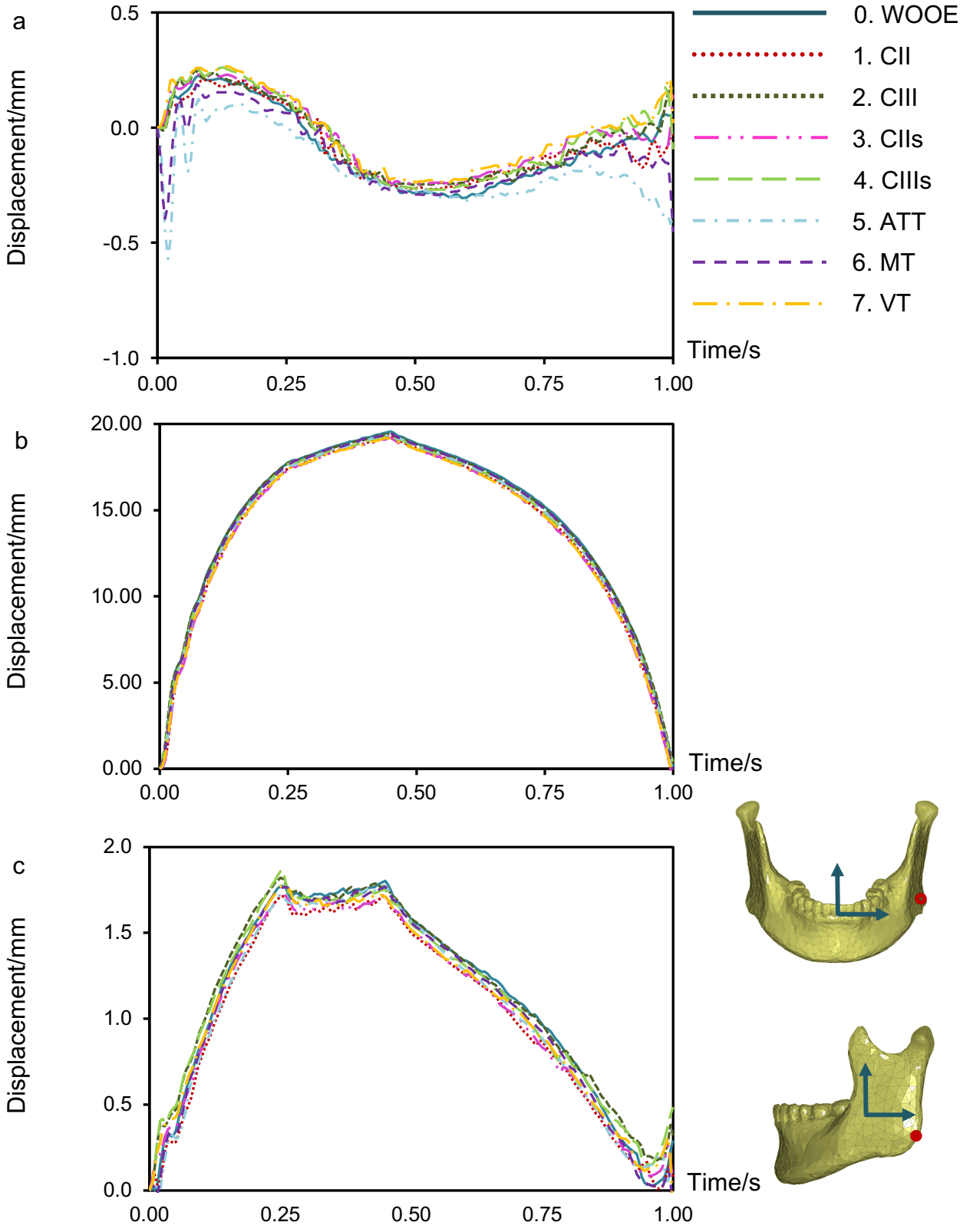

Figure 20: Displacement of the reference node left Go of the 8 models. (a) X-axis (b) Y-axis (c) Z-axis.

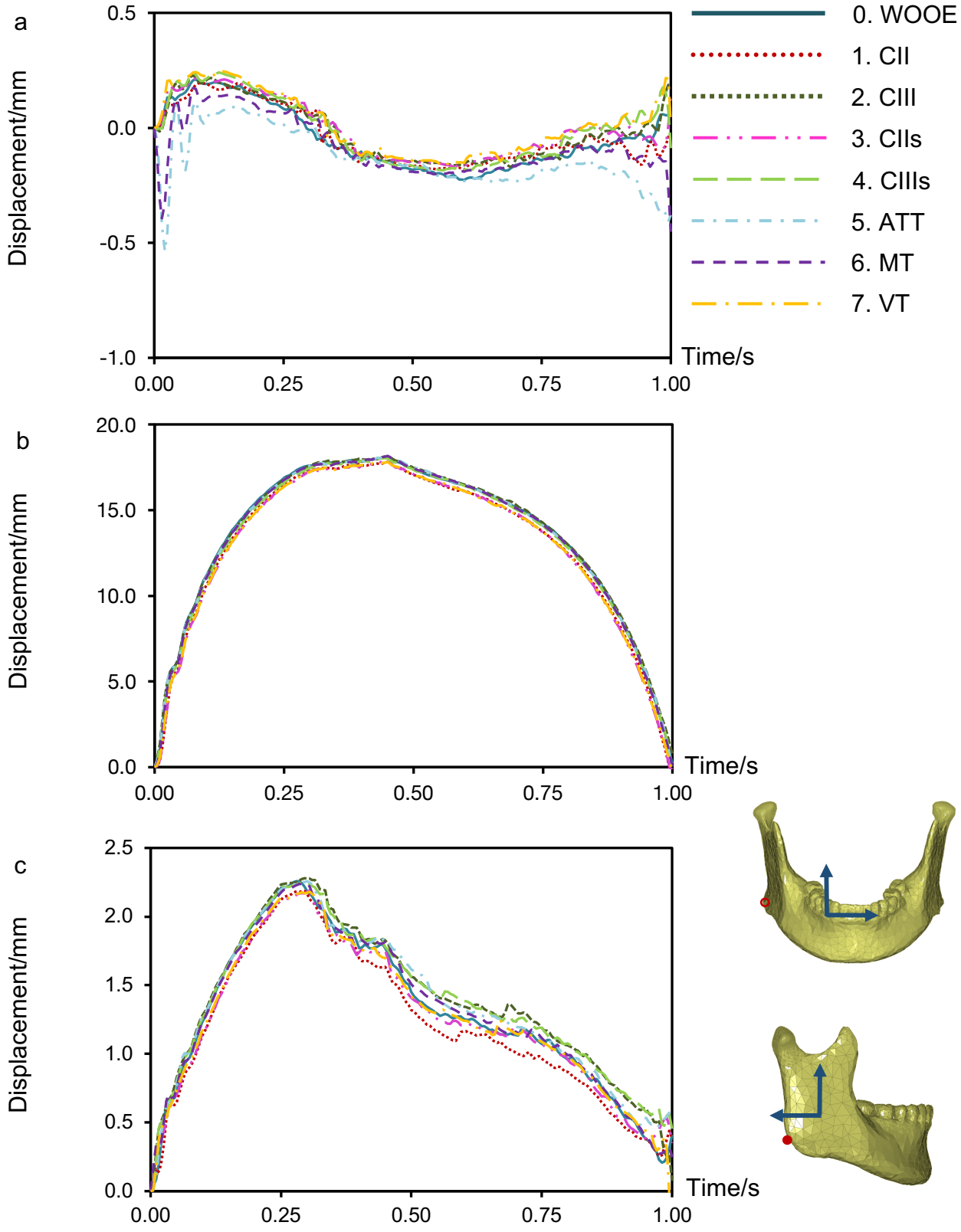

Figure 21: Displacement of the reference node right Go of the 8 models. (a) X-axis (b) Y-axis (c) Z-axis.

Figure 24 shows the MaxPS in the discs of the eight models at full mouth opening. The patterns of distribution of the stresses were highly similar among the models. Based on the display of colours, the magnitudes of stresses in the major area of the discs were close nevertheless; the maximum tensile stresses and minimum compressive stresses were different. The extrema of MaxPS in discs was illustrated as bar graphs in Figure 25, the positive side represents tensile stress, and the negative side represents compressive stresses. The highest tensile stress in the left disc was 36.6 MPa, produced from Model MT, while the lowest one was 32.9 MPa, from Model CIIs. On the right side, the highest tensile stress was from Model CIII (37.6 MPa), and the lowest was from Model MT (18.0 MPa).

The highest compressive stress in the left discs was from Model CII (-17.3 MPa), and the lowest was -29.1 MPa, from Model CIIs. On the right side, the highest compressive stress was -30.3 MPa, from Model VT, and the lowest was from Model CIIIs, which was -43.64 MPa. Compared with the MaxPS in discs of Model WOOE (29.2 MPa), tensile stresses in the right discs of Model ATT and Model MT (18.5 and 18.0 MPa respectively) were significantly smaller. Meanwhile, the compressive stress in the left disc of Model CII (-17.3 MPa) was significantly larger than Model WOOE (-28.2 MPa).

Figure 26 shows the MaxPS in the condylar cartilage of the eight models at the full mouth opening. The patterns of the stress distribution were also highly similar among the models, but the magnitudes of the compressive stresses were different. Figure 27 shows the extrema of MaxPS in the condylar cartilage. The compressive stresses were relatively similar to that of the disc, but the tensile stresses were much smaller. It denotes that among all the models, the highest tensile stress in the left disc was 5.0 MPa, from Model CII, and the lowest was 2.7 MPa, from Model VT. On the right, the highest tensile stress was from Model VT (5.0 MPa), and the lowest was from Model WOOE (3.0 MPa). The highest compressive stress in the left disc was from model CII (-18.2 MPa), which was significantly larger than the one of Model WOOE (-30.4 MPa) while, the lowest was from Model CIIs (-32.5 MPa). On the right side, the highest compressive stress was from Model CIIs (-31.2 MPa), and the lowest was from Model CIII (-45.5 MPa).

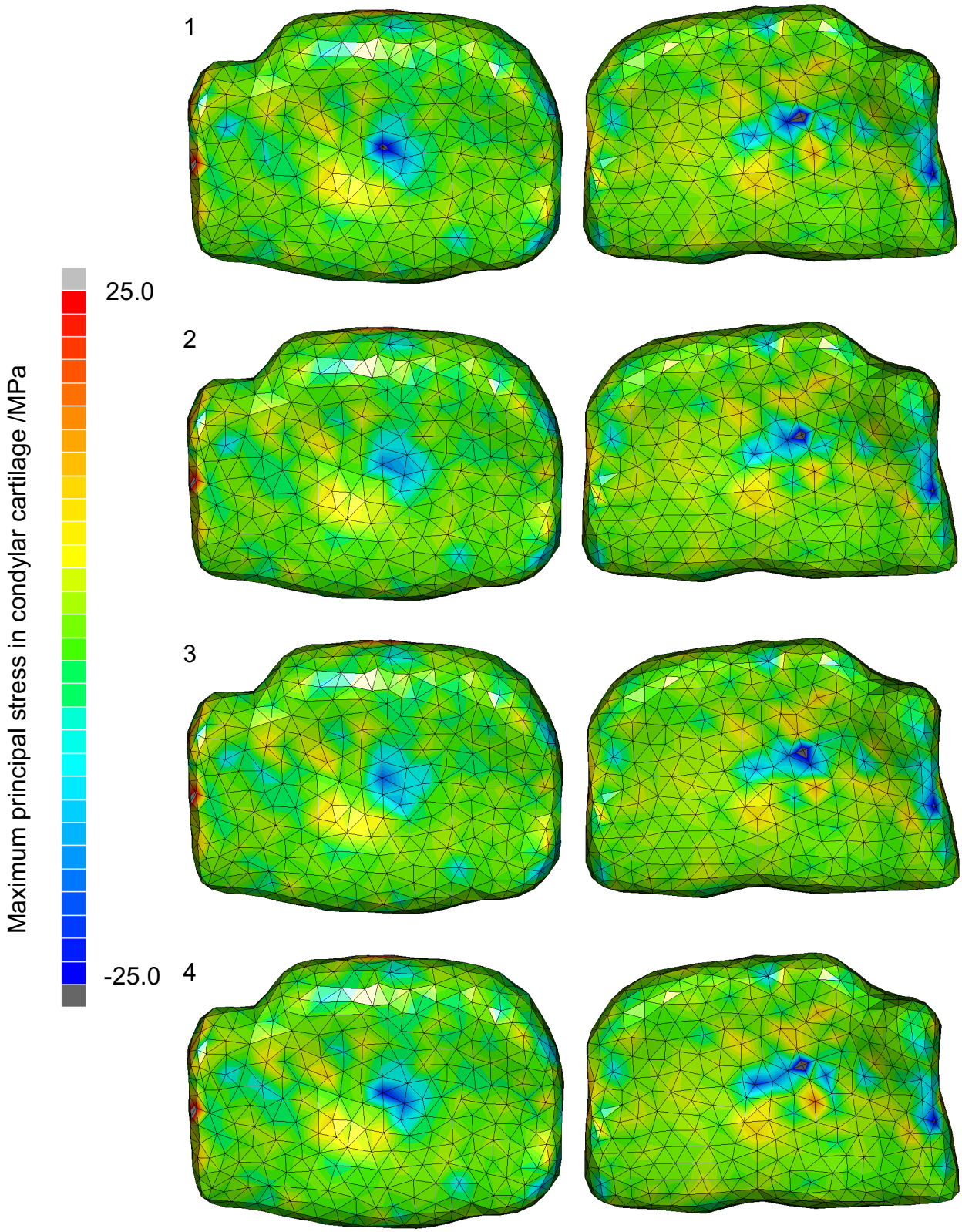

Figure 22a: Distribution and magnitude of the maximum principal stress on the surface of the left and right articular disc. (1) Model WOOE (2) Model CII (3) Model CIII (4) Model CIIIs

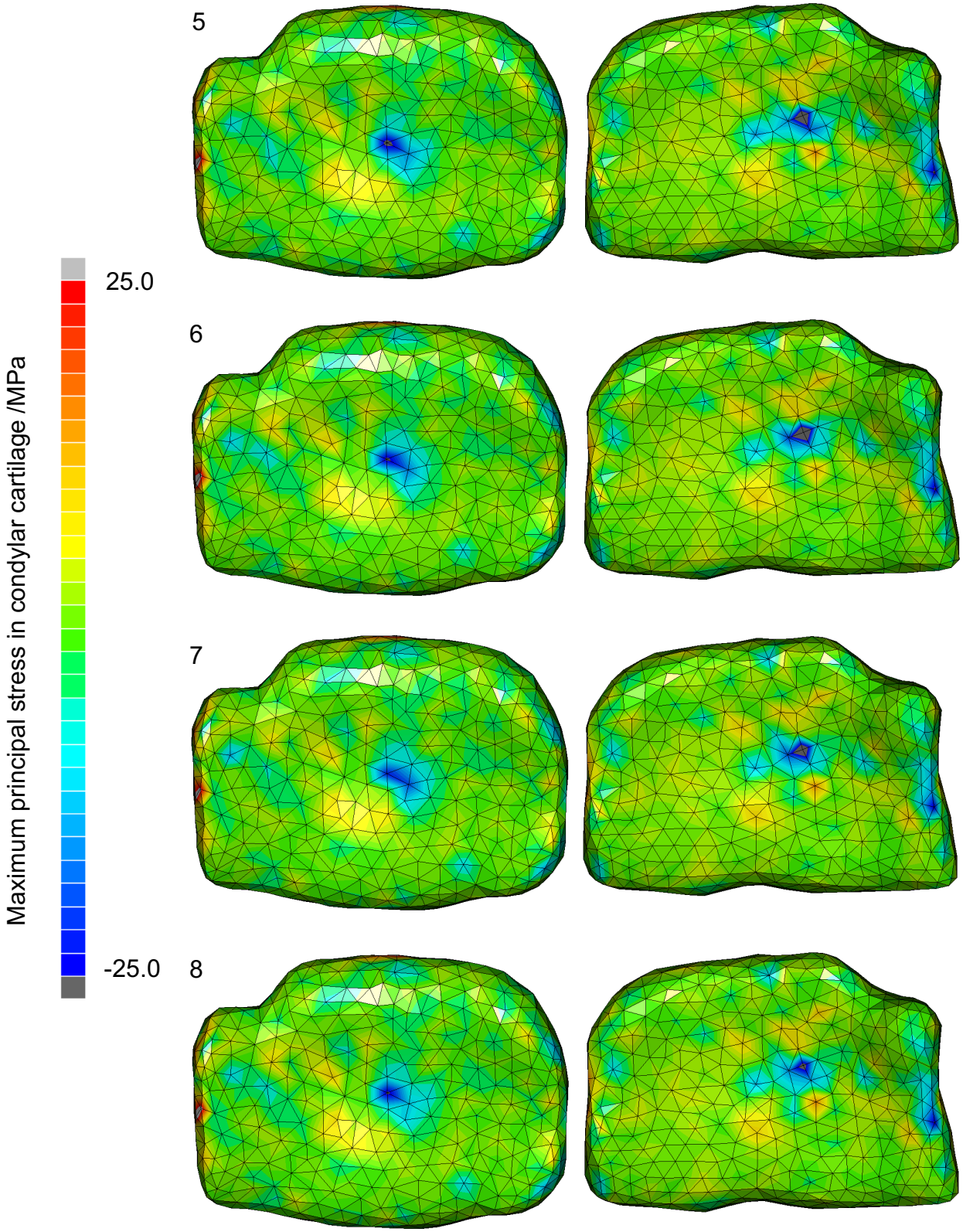

Figure 24b: Distribution and magnitude of the maximum principal stress on the surface of the left and right articular disc. (5) Model CIIIs (6) Model ATT (7) Model MT (8) Model VT

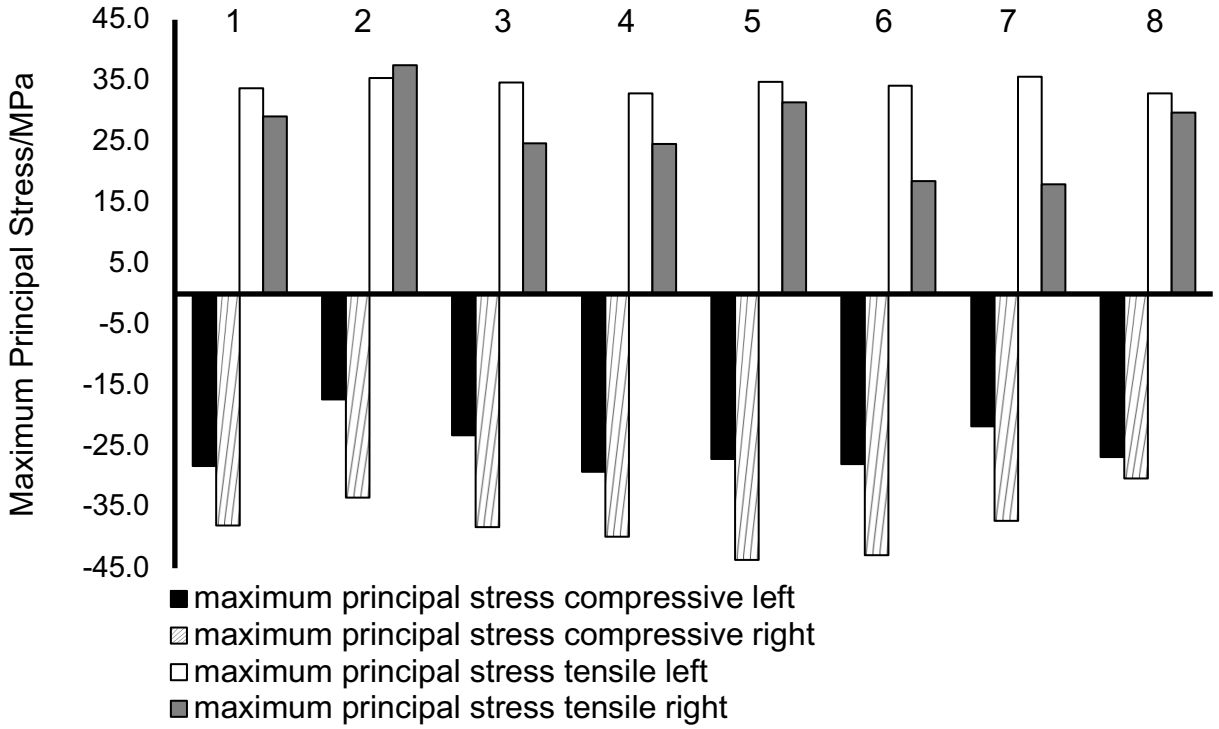

Figure 23: The extrema of maximum principal stress in the discs and at full mouth opening. (1) Model WOOE (2) Model CII (3) Model CIII (4) Model CIIIs (5) Model CIIIs (6) Model ATT (7) Model MT (8) Model VT

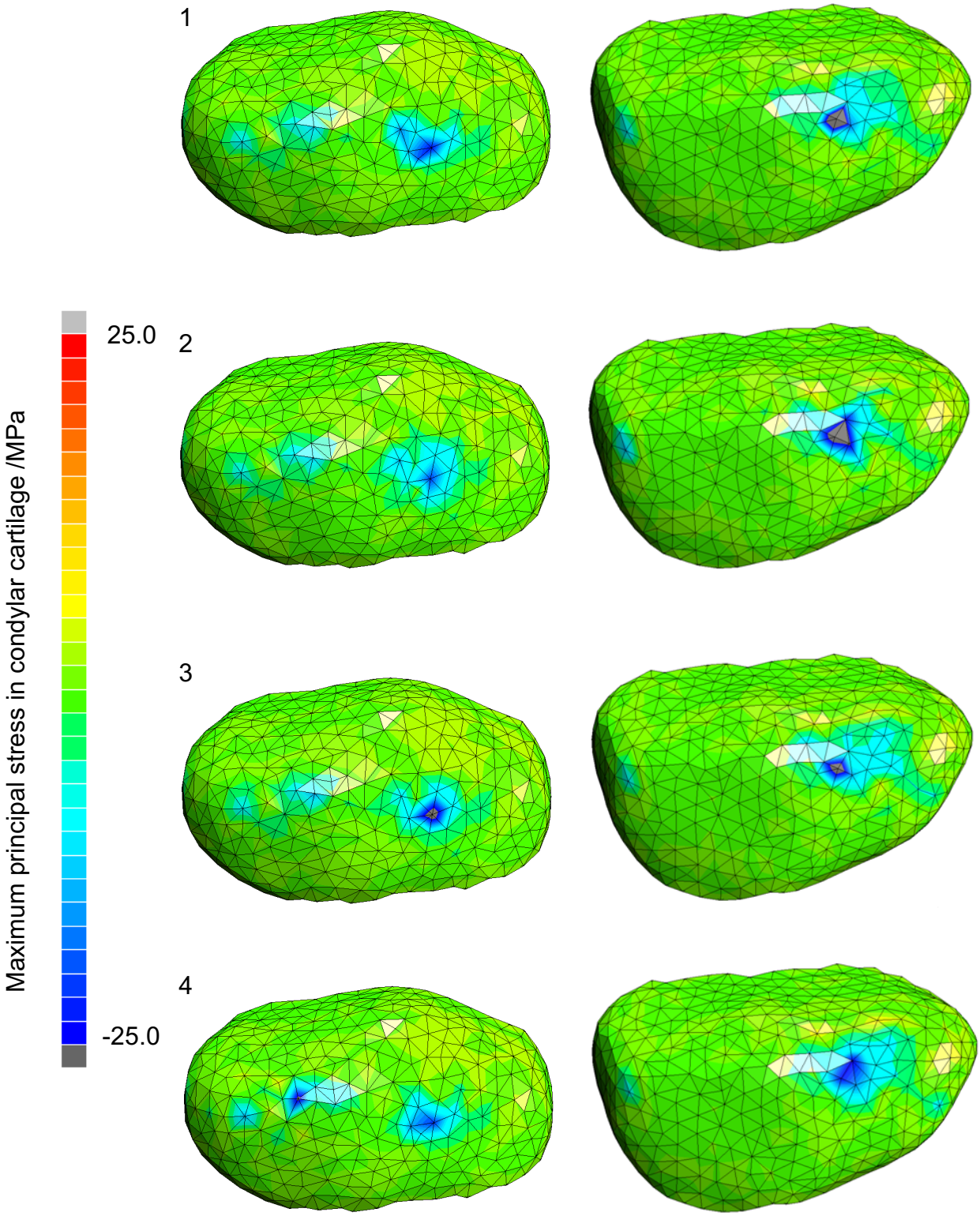

Figure 24a: Distribution and magnitude of the maximum principal stress on the surface of the left and right condylar cartilage. (1) Model WOOE (2) Model CII (3) Model CIII (4) Model CIIIs

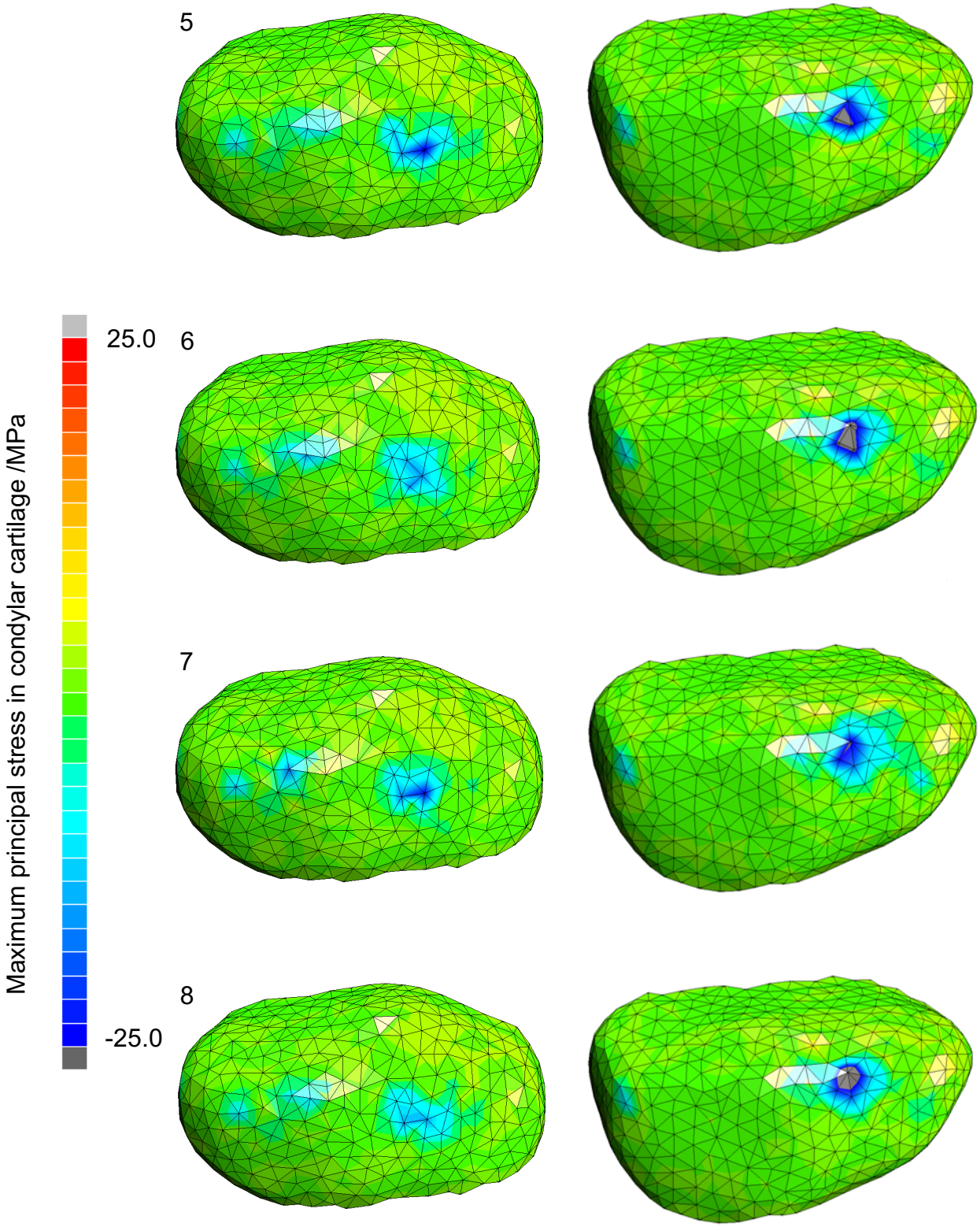

Figure 26b: Distribution and magnitude of the maximum principal stress on the surface of the left and right condylar cartilage. (5) Model CIIIs (6) Model ATT (7) Model MT (8) Model VT

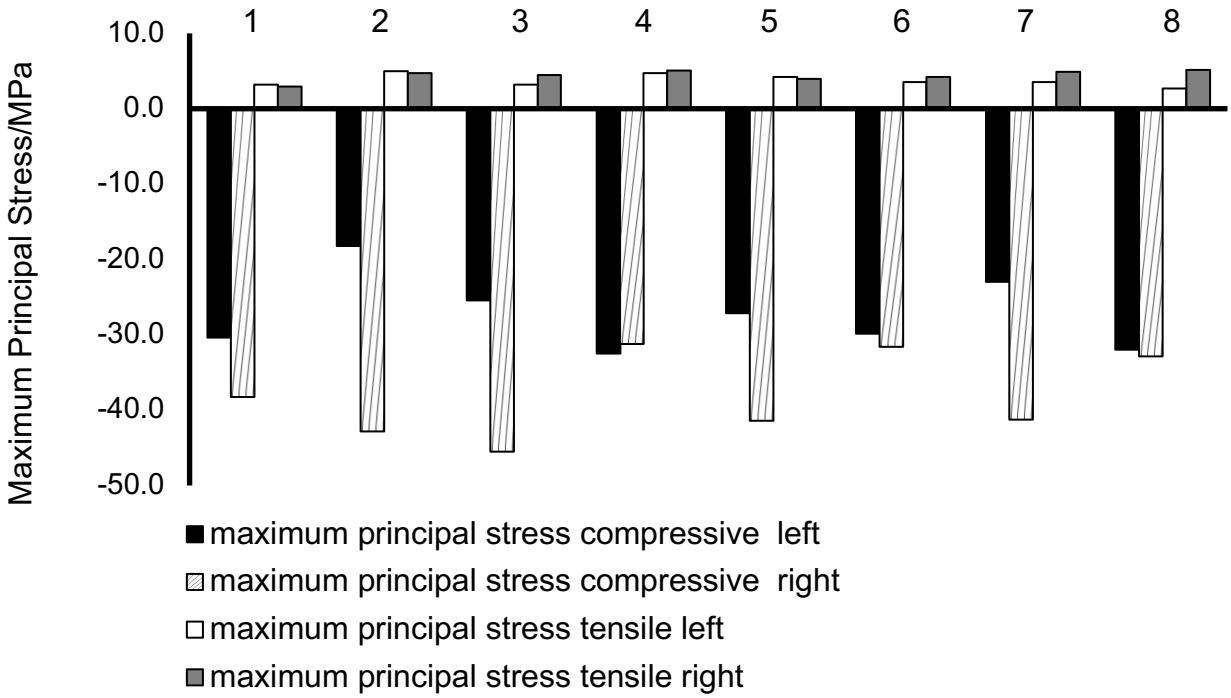

Figure 25: The extrema of maximum principal stress in the articular cartilage at full mouth opening. (1) Model WOOE (2) Model CII (3) Model CIII (4) Model CIIIs (5) Model CIIIs (6) Model ATT (7) Model MT (8) Model VT

5. Discussion

5.1 General discussion of FE model

Our model included the whole skeletal skull, except for the top and back of the head, because of the limitation of the CT image. For simplification and ease of calculation, some anatomical structures were not included in our model, such as the ligaments of the border movement of the mandible, muscles of facial expression, vessels, nerves and skin, etc. The roots of teeth and the periodontal ligament were excluded as well and the extensibility of the latex elastics were not considered either. The OEs are generally applied when the teeth are aligned. During this treatment, both upper and lower teeth are bonded and fixed with stiff steel edgewise arch wire and ligature wires, to integrate the teeth and the corresponding jaw for occlusion adjustments.

The present biomechanical masticatory system model with TMJ is capable to simulate varieties of oral activities, as well as diverse therapeutic approaches. The distribution and magnitude of stresses in the articular disc (AD), condylar cartilage and the kinematic parameters of the mandible can be directly visualised and measured through the postprocessor of MSC.Marc/Mentat. In in vivo studies, due to individual differences and the complexity of human biological systems, there is a wide range of expected or unexpected variables that cannot be controlled. While in FE simulation, this problem can be solved by using the same basic FE model with changing between the different variables. Since the FE model was created based on patient-specific geometry, the individual difference cannot be neglected and the calculated stress value should only be used for comparative studies (Sagl et al., 2019).

Since 1978, the function of the TMJ was verified as a loading process on macaque, and the biomechanical behaviour of TMJ was widely studied through different methods (Brehnan et al., 1981; Hylander and Bays, 1979). Overloading of the TMJ was presented as a risk factor for TMD, and it was suggested that when the orthopaedic force surpasses the physiologic tolerance, the risk of TMD will be increased or the symptoms of TMD will be worse (Farrar and McCarty, 1982; Serbesis-Tsarudis and Pancherz, 2008; Wyatt, 1987). Since the biomechanical effect of the intermaxillary elastics to TMJ is still not well studied, the evidences to support the relationship between TMD and OEs are still not sufficient. To our knowledge, previous models that studied the effect of orthodontic traction

on the TMJ were static models only. Thus, this study might be the first dynamic simulation with including asymmetric traction as well. It aimed to provide a better understanding of the biomechanical mechanisms of OEs on the TMJ and to provide some ideas for clinical treatment.

5.2 Material properties

The human TMJ disc demonstrates biphasic viscoelastic properties owing to its biochemical composition. Also because of the variations in biochemical composition and the irregular structure, the dynamic biomechanical behaviour of the disc in the anterior, posterior band and intermediate zone are also different (Kuo et al., 2010). The Mooney-Rivlin model was used in this study because it is relatively less complicated and widely used in literature. A sensitivity analysis of the material parameters showed that the dynamic behaviour of the mandible is not remarkably sensitive to the changing of the constants C1 and C2 of the material model (Sagl et al., 2019). Furthermore, the material properties of cartilaginous structures are mainly animal-sourced, from porcine, in all the three material models above. Kuo et al. (2010) collected 12 fresh left discs from cadavers and did a biphasic viscoelastic properties test in the five regions of the discs under confined compression. The equilibrium aggregate modulus, hydraulic permeability and dynamic modulus of the five regions of the discs were obtained, but these parameters are not utilized in the simulation yet.

5.3 Discussion of the results

5.3.1 Validation of the reference model

The computed mouth opening reached the largest inter-incisal gap in 0.45 s and closed in 0.55 s. 1 Hz of mouth opening and closing frequency reflect human masticatory conditions (Gallo et al., 2000; Tanaka et al., 2004). The condyles mainly rotated in the first 0.25 s, after the inter-incisal gap reached 25 mm, they rotated while translating forward along the posterior slope of the glenoid process. At the end, a 30 mm inter-incisal gap was obtained at full mouth opening, which agrees with the in vivo study of kinematics of human mandible and previous simulation studies (Koolstra and van Eijden, 2005; Langenbach and Hannam, 1999; Motzko et al. 2019; Sagl et al., 2019; Visscher et al., 2000). In in vivo studies, with the assistant of the backward rotation of the head and the caudal translation

of the hyoid bone, the inter-incisal gap can reach 50 mm. While considering the extreme mouth opening is not that common in daily life, we simplified the simulations by excluding the actions of head and hyoid bone. The displacement of the five reference nodes on the x-axis displayed slight asymmetrical movement of the mandible. This might be caused by the structural asymmetry or the orientations of the muscles on sides of the facial middle line. According to the trend and the colours of the arrows in Figures 13 and 14, this asymmetry barely affected the general mandibular movement.

At full mouth opening, the compressive stress was primarily concentrated in the middle of the intermediate zone of the disc. The relatively lower tensile stress was dispersedly around the compressive stress on the disc, and the high tensile stress distributed on the anterior and medial side of the disc. In condylar cartilage, the compressive stress distributed mainly on the anterior slope of the condylar head, relatively leftward on both condyles. This could be attributed to the slight asymmetrical translation on the x-axis mentioned above.

Generally, the distribution of stresses was consistent with the anatomical structure and physiological behaviour of the TMJ. The compressive stress in discs and cartilage was comparable, while the tensile stress in the cartilage was much lower than that of discs (almost one order of magnitude lower), and this is consistent with previous studies (Koolstra and van Eijden, 2005). The cartilage has a very limited stretching capability because it is fixed to the skeletal condyle beneath it, while the disc is much freer to deform. That is why biologically the disc is located between the condyle and the glenoid fossa and is acting as a cushion to buffer the impact from the motion.

In the present study, the magnitude of MaxPS at full mouth opening is similar to the result of FE study from Koolstra et al. however; two orders of magnitude were higher than the results of Sagl et al. (Koolstra and van Eijden 2005; Sagl et al., 2019). Results of these former two investigations were used for comparison in the present study because the adopted material properties and the muscle model were similar. Moreover, any slight differences could be attributed to the variance in the program built-in algorithms or classes of the elements. With tetrahedron elements of cartilaginous structures, the magnitude of MaxPS was similar to the results of Sagl et al. (2019), but there was an obvious penetration between the deformable tissues, cartilage and disc during the mandibular movement.

To eliminate the penetration, we tested tetrahedron elements with the Segment-to-segment contact method (the contact method in default is Node-to-segment), or with the Node-to-segment method when the simulation failed to converge in very early steps. Considering this could be due to the geometric nature of tetrahedral elements, we tested hexahedral elements for all largely deformable structures and finally obtained a stable simulation without penetrations among the cartilaginous structures.

5.3.2 Comparison of the results

The kinematic characters of the eight models were highly similar in pattern or magnitude except for the displacement on the x-axis of the models with molar and anterior teeth traction. Due to the effect of the asymmetrical elastics, at the early stage of the mouth opening, the mandible was pulled towards the left, which was the anchorage side (significant displacement on the negative x-axis). On increasing the amplitude of the masticatory muscles, the asymmetry was rectified. Moreover, the time-displacement curves of gnathion and gonions on the x-axis of models ATT and MT were under the curves of all the other models, while this did not happen to condylions.

Based on the results, we can conclude that the OEs have more influence on the mandibular body rather than the condyles. This also supports the general opinion that orthodontic correction is achieved through dento-alveolar change rather than TMJ remodelling (Serbesis-Tsarudis and Pancherz, 2008). According to the contour band graphic, the distributing pattern of stresses in the discs and cartilage of the eight models were highly similar at the full mouth opening. This was also proved by the resemblance of the kinematic characters of the mandible.

The elastic force at full mouth opening could reach around 2.5 times larger than its starting load, while the stress in the discs with OEs was not large in magnitude compared with Model WOOE. Although it is clear that the stress in some of the models with OEs was significantly small, the result of the left and right sides from the same model did not show any consistency. Hence, the conclusion that OEs can alleviate the stress in the cartilaginous structures cannot be simply drawn either.

5.3.3 Clinical conclusions

Based on the results, symmetrical OEs did not significantly influence the mandibular kinematic trajectory and the stress in cartilaginous tissues of the TMJ. Non-symmetrical OEs influences the mouth opening at the early stage but did not increase the stress in the cartilaginous tissues of TMJ. Therefore, it is not postulated that the medium orthodontic elastic force would cause harmful effects on healthy TMJ. Furthermore, the slight effect on the rotation of the mandible resulting from Class II and Class III OEs could be identified. The Class II OEs led the clockwise trend of the mandible, while the Class III OEs led the counter- clockwise trend of the mandible. This effect is beneficial to certain corresponding cases in the clinic.

Humans maintain an upright head or body posture most time of the day, so the mandible is in a resting position. There is 1-3 mm space between upper and lower front teeth in this condition unconsciously, with slight activation of the elevator muscles to overcome the weight of the mandible. Meanwhile the disc is in a neutral position, and there is superior and inferior joint space above and under the disc, so the stress in the disc or the articular cartilage is little (Motzko et al. 2019). Consequently, the resting posture has important biological meaning for the health of TMJ.

In the present study, the cbCT of the geometry that we adopted was taken at intercuspation of the subject, and the computed mouth opening began from this mandibular position. Some researchers found that the mandibular rest position varied widely, even with oneself at a different time of the day and under different mental and physical conditions. (Tingey et al., 2001). In an investigation of the role of passive force of masticatory muscles with the FE method, it was found that the mandibular rest position needed 0.2 % activation of the elevator muscles (Langenbach and Hannam, 1999). From this literature, we could estimate that the composition of forces of 0.2 % of the elevators is 1.55 N, and it could overcome the 200 g mass of the mandible to preserve the resting posture. In another FE study, they activated 0.08% of elevator muscles (0.62 N) to overcome the 400 g mass of the mandible to achieve a rest position (Sagl et al., 2019). The force of OE in the present study is around 1.25 N, whether it is large enough to close the mouth is a question that we should consider. Because it might increase the stress on the posterior band of the disc when the mouth is closed (the molars contact), and the patient will feel tired after a long time in this condition (Dawson, 2007). Moreover, it is not only the magnitude of the force

but also the moment of the force that define the position of the mandible. The mandibular rotational centre is on the condyle and horizontally to the medial pole with an initial mouth opening (the increment of inter-incisor gap< 25 mm) (Dawson, 2007; Motzko et al. 2019). The moment of OE force is different depending on the force application point of different OEs. Hence, the investigation of the stress caused by OE on TMJ disc at mandibular rest position is still needed, this is planned to a continuation of our work in the future.

6. Summary

The Finite element method was used to investigate whether variations of intermaxillary elastics would develop harmful effects on the healthy temporomandibular joint. The biomechanical behaviour of computed dynamic mouth opening and closing without and with seven configurations of orthodontic intermaxillary elastics were analysed. We developed a finite element model with a masticatory system based on anonymised CT and MRI scans using Mimics and MSC.Marc/Mentat software. Subjects were individuals with normal occlusion and without temporomandibular disorder. The two six-degree-of-freedom temporomandibular joints consisted of articular cartilage, disc, discal ligament and retrodiscal lamina. Twelve pairs of muscles approximated by Hill-type point-to-point actuators were employed to move the mandible.

The material properties of cartilaginous tissues were considered as Mooney-Rivlin material model. The simulated kinematic behaviour of mouth opening and closing without orthodontic intermaxillary elastics was consistent with numerous in vivo studies. The compressive stress was mainly at the intermediate zone of the disc and the anterior slope of the condylar process on full mouth opening. With around 1.25 N medium intermaxillary elastics initial load at intercuspation, the distribution of the maximum principal stresses in the discs of the models with and without elastics at full mouth opening were quite similar. Compared with the simulation without elastics, the tensile and compressive stresses in the discs with different intermaxillary elastics were not significantly larger. In some simulations with elastics, the tensile or compressive stress was significantly smaller, but there was no regulation of the difference, according to the value of the left and right sides. It is the same with the stresses in the condylar cartilage, and they were comparable with the stresses in the discs. This is consistent with previous studies. In general, the movement of the mandible without and with seven configurations of elastics was highly alike in pattern and magnitude. This also supported the resemblance of the distribution of stresses on the surface of the discs and condylar cartilage.

In the results of non-symmetrical elastics simulations, molar traction and anterior teeth traction, there was obvious displacement in the negative direction on the x-axis, before 0.06s. This means that the mandible moved toward the anchorage side at the early stage

of mouth opening, but this was corrected after a few steps as the amplitude of the mouth depressor muscles increased.

The finite element model of TMJ including the masticatory system helped us to observe and analyse the biomechanical behaviour of the joint during functional loading. Orthodontic intermaxillary elastics did not significantly influence the distribution and magnitude of the stress in cartilaginous tissues, and the kinematic behaviour of the mandible. In general, the present finite element model can help to analyse the relationship between temporomandibular joint and therapeutic approaches in the clinic. Nevertheless, due to the individual diversities, the complex material properties of the cartilaginous tissues and dynamic masticatory behaviour, the computed result is only advocated as a reference for the clinic treatment.

7. List of figures

8. List of tables

9. References

Al-Saleh MAQ, Alsufyani N, Flores-Mir C, Nebbe B, Major PW. Changes in temporomandibular joint morphology in class II patients treated with fixed mandibular repositioning and evaluated through 3D imaging: A systematic review. Orthod Craniofacial Res 2015; 18: 185-201

Aoyama J, Tanaka E, Miyauchi M, Takata T, Hanaoka K, Hattori Y, Sasaki, A, Watanabe, M, Tanne, K. Immunolocalization of vascular endothelial growth factor in rat condy- lar cartilage during postnatal development. Histochem Cell Biol 2004; 122: 35-40

Ash MM, Nelson SJ. In: Dolan JJ, Loehr BS eds., Wheeler's Dental Anatomy, Physiology and Occlusion: London, Elsevier Inc., 2010

Beatty MW, Nickel JC, Iwasaki LR, Leiker M. Mechanical response of the porcine temporomandibular joint disc to an impact event and repeated tensile loading. J Orofac Pain 2003; 17:160-166

Beek M, Koolstra JH, van Ruijven LJ, Van Eijden TMGJ. Three-dimensional finite element analysis of the cartilaginous structures in the human temporomandibular joint. J Dent Res 2001; 80: 1913–1918

Beek M, Koolstra JH, van Eijden TMGJ. Human temporomandibular joint disc cartilage as a poroelastic material. Clin Biomech 2003; 18: 69-76

Boyd, RL, Gibbs, CH, Mahan, PE, Richmond, AF, Laskin, JL. Temporomandibular joint forces measured at the condyle of Macaca arctoides. Am J Orthod Dentofacial Orthop 1990; 97: 472-479

Brehnan K, Boyd RL, Laskin J, Gibbs CH, Mahan P. Direct Measurement of Loads at the Temporomandibular Joint in Macaca arctoides. J Dent Res 1981; 60: 1820–1824

Breitner C. Bone changes resulting from experimental orthodontic treatment. Am J Orthod Oral Surg 1940; 26: 521–547

Chisnoiu AM, Picos AM, Popa S, et al. Factors involved in the etiology of temporomandibular disorders - a literature review. Clujul Med 2015; 88: 473-478.

de Clerck H, Nguyen T, de Paula LK, Cevidanes L. Three-dimensional assessment of mandibular and glenoid fossa changes after bone-anchored Class III intermaxillary traction. Am J Orthod Dentofac Orthop 2012; 142: 25–31

Commisso MS, Martínez-Reina J, Mayo J. A study of the temporomandibular joint during bruxism. Int J Oral Sci 2014; 6: 116-123

Commisso MS, Ojeda J, Mayo J, Martínez-Reina J. Influence of the Temporomandibular Joint in the Estimation of Bone Density in the Mandible through a Bone Remodelling Model. Math Probl Eng 2018; 2018

Costen JB. A syndrome of ear and sinus symptoms dependent upon disturbed function of the temporomandibular joint. Ann Otol Rhinol Laryngol 1997; 106:805-819

Dawson PE. In: Dolan, J, Nebel J eds., Functional Occlusion: From TMJ to Smile Design: St. Louis, Mosby Elsevier 2007

Detamore MS, Athanasiou KA. Motivation, characterization, and strategy for tissue engineering the temporomandibular joint disc. Tissue Eng 2003; 9:1065-1087

Dibbets JMH, van der Weele LT. Long-term effects of orthodontic treatment, including extraction, on signs and symptoms attributed to CMD. Eur J Orthod 1992; 14: 16–20

van Eijden TMGJ, Korfage JAM, Brugman P. Architecture of the human jaw-closing and jaw-opening muscles. Anat Rec 1997; 248: 464-474

Farrar WB, McCarty WL. A clinical outline of temporomandibular joint diagnosis and treatment. Normandie Publications, Montgomery, 1982

Garcia E, Leal MM, Villamil MB. Modeling and simulation of masticatory muscles. Procedia Comput Sci 2015; 51: 2878–2882

Gallo LM, Nickel JC, Iwasaki, LR, Palla, S. Stress-field translation in the healthy human temporomandibular joint. J Dent Res 2000; 79: 1740-1746

Greaves, WS. The jaw lever system in ungulates: a new model. J Zool 1978; 184: 271-285

Gurbanov V, Bas B, Öz AA. Evaluation of Stresses on Temporomandibular Joint in the Use of Class II and III Orthodontic Elastics: A Three-Dimensional Finite Element Study. J Oral Maxillofac Surg 2020; 78: 705-716

Gysi A. Studies on the leverage problem of the mandible. Dent Digest 1921; 27: 74-84, 144-150, 203-208

Hasan I, Röger B, Heinemann F, Keilig L, Bourauel C. Influence of abutment design on the success of immediately loaded dental implants: experimental and numerical studies. Med Eng Phys 2012; 34: 817-825

Hasson T, Öberg T, Carlsson GE, Kopp S. Thickness of the soft tissue layers and the articular disk in the temporomandibular joint. Acta Odontologica Scandinavica 1997; 35: 77-83

Haskell B, Day M, Tetz J. Computer-aided modelling in the assessment of the biomechanical determinants of diverse skeletal patterns. Am J Orthod 1986; 89: 363–382

Hatcher DC, Faulkner MG, Hay A. Development of mechanical and mathematic models to study temporomandibular joint loading. J Prosthet Dent 1986; 55:377-384

Hayes WC, Bodine AJ. Flow-independent viscoelastic properties of articular cartilage matrix. J Biomech 1978; 11:407-419

Herring SW, Decker JD, Liu ZJ, Ma T. Temporomandibular joint in miniature pigs: Anatomy, cell replication, and relation to loading. Anat Rec 2002; 266: 152–166

Henrikson T, Milner M. Temporomandibular disorders, occlusion, and orthodontic treatment. Journal of Orthodontics 2003; 30: 129-137

Hill, AV. The heat of shortening and the dynamic constants of muscle. Proceedings of the Royal Society B 1938; 126: 136-195

Hill, AV. The mechanics of active muscle. Proceedings of the Royal Society of London. Series B 1953; 141: 104-117

Hiraba K, Hibino K, Hiranuma K, Negoro T. EMG activities of two heads of the human lateral pterygoid muscle in relation to mandibular condyle movement and biting force. J Neurophysiol 2000; 83: 2120–2137

Hylander, WL, and Bays R. An in vivo strain-gauge analysis of the squamosal-dentary joint reaction force during mastication and incisal biting in Macaca mulatta and Macaca fascicularis. Archives of Oral Biology 1979; 24: 689-697

Klein B. In: Zipsner T eds., FEM: Grundlagen und Anwendungen der Finite-Element-Methode im Maschinen- und Fahrzeugbau: Wiesbaden, Vieweg und Teubner Verlag, 2012: 9

Keilig L. Experimentelle und numerische Untersuchungen zum Verschleiß von Halteelementen in der zahnärztlichen Prothetik. Dissertation paper from the Mathematics and Natural Science Faculty of the University of Bonn (2008)

Hexagon Manufacturing Intelligence, 2021: Marc 2021.1 Volume A: Theory and User Information. https://help.hexagonmi.com/bundle/Marc_2021.1-Volume_A_Theory_and_User_Information/resource/Marc_2021.1-Volume_A_Theory_and_User_Information.pdf (date of access: 04.07.2022)

Koolstra JH, van Eijden TMGJ. Biomechanical Analysis of Jaw-closing Movements. J Dent Res 1995; 74: 1564–1570

Koolstra JH, van Eijden TMGJ. The jaw open-close movements predicted by biomechanical modelling. J Biomech 1997; 30: 943–950

Koolstra JH, van Eijden TMGJ. Combined finite-element and rigid-body analysis of human jaw joint dynamics. J Biomech 2005; 38: 2431-2439

Koolstra JH, van Eijden TMGJ. Prediction of volumetric strain in the human temporomandibular joint cartilage during jaw movement. J Anat 2006; 209: 369-380

Kumar N, Adhikari R, Anjaiah D, Marimuthu R. Finite Element Analysis Using Herrmann Formulation for Viscoelastic Materials. Intl. Conf. on Advances in Civil, Structural and Mechanical Engineering 2015; 2: 59-63

Kuo J, Zhang L, Bacro T, Yao H. The region-dependent biphasic viscoelastic properties of human temporomandibular joint discs under confined compression. J Biomech 2010; 43: 1316-1321

Kuroda S, Tanimoto K, Izawa T, Fujihara S, Koolstra JH, Tanaka E. Biomechanical and biochemical characteristics of the mandibular condylar cartilage. Osteoarthr Cartil 2009; 17: 1408–1415

Langenbach GEJ, Hannam AG. The role of passive muscle tensions in a three-dimensional dynamic model of the human jaw. Arch Oral Biol 1999; 44: 557-573.

de Leeuw R. In: Klasser GD eds., Orofacial pain: guidelines for assessment, diagnosis, and management: Hanover Park, Quintessence Publishing Company, 2018

de Leeuw, R. Orofacial pain; guidelines for assessment, diagnosis, and management, 4th ed, 2008

Luder HU, Leblond CP, von der Mark K. Cellular stages in cartilage formation as revealed by morphometry, radioautography and type II collagen immunostaining of the mandibular condyle from weanling rats. Am J Anat 1988; 182: 197–214

Luther F. TMD and occlusion part I. Damned if we do? Occlusion: The interface of dentistry and orthodontics. Br Dent J 2007; 202: 1-7

Mao JJ, Rahemtulla F, Scott PG. Proteoglycan expression in the rat temporomandibular joint in response to unilateral bite raise. J Dent Res 1998; 77: 1520-1528

Martins JAC, Pires EB, Salvado R, Dinis PB. A numerical model of passive and active behavior of skeletal muscles. Comput Methods Appl Mech Eng 1998; 151: 419-433

Meissner U, Maurial A. Die Methode der finiten Elemente. Berlin - Heidelberg: Springer Verlag, 2000

Michelotti A, Iodice G. The role of orthodontics in temporomandibular disorders. J Oral Rehabil 2010; 37: 411-429

Mizoguchi I, Takahashi I, Nakamura M et al. An immunohistochemical study of regional differences in the distribution of type I and type II collagens in rat mandibular condylar cartilage. Arch Oral Biol 1996; 41: 863–869

Mooney M. A theory of large elastic deformation. J Appl Phys 1940; 11: 582–592

Motzko M, Weinert M, Albrecht U. Kiefergelenk und Kaustörungen: Berlin, Springer 2019

Mow VC, Ateshian GA, Spilker RL. Biomechanics of diarthrodial joints: a review of twenty years of progress. J Biomech Eng 1993; 115: 460-467

Murphy MK, MacBarb RF, Wong ME, Athanasiou KA. Temporomandibular Disorders: A Review of Etiology, Clinical Management, and Tissue Engineering Strategies. Int J Oral Maxillofac Implants 2013; 28: e393-e414

Okeson JP. Long-term treatment of disk-interference disorders of the temporomandibular joint with anterior repositioning occlusal splints. J Prosthet Dent 1988; 60: 611-616

Owtad P, Park JH, Shen G, Potres Z, Darendeliler MA. The biology of TMJ growth modification: A review. J Dent Res 2013; 92: 315-321

Peck CC, Langenbach GEJ, Hannam AG. Dynamic simulation of muscle and articular properties during human wide jaw opening. Arch Oral Biol 2000; 45: 963-982

Pollack B. Cases of note. Michigan jury awards $850,000 on ortho case: a tempest in a teapot. Am J Orthod Dentofacial Orthop 1988; 94: 358-360

Proffit WR, Fields H, Sarver DM. Contemporary Orthodontics. 5th ed. Linda Duncan: St. Louis, 2013

Rivlin RS. Torsion of a rubber cylinder. J Appl Phys 1947; 18: 444–449

Roda RP, Díaz Fernández JM, Hernández Bazán S, Jiménez Soriano Y, Margaix M, Sarrión G. A review of temporomandibular joint disease (TMJD). Part II: Clinical and

radiological semiology. Morbidity processes. Med Oral Patol Oral Cir Bucal 2008a; 13: 102-109

Roda PR, Fernández JMD, Bazán SH, Soriano YJ, Margaix M, Sarrión G. A review of temporomandibular joint disease (TMJD). Part II: Clinical and radiological semiology. Morbidity processes. Med Oral Patol Oral Cir Bucal 2008b; 13: 102–109

Sagl B, Schmid-Schwap M, Piehslinger E, Kundi M, Stavness I. A Dynamic Jaw Model with a Finite-Element Temporomandibular Joint. Front Physiol 2019; 10: 1-12

Serbesis-Tsarudis C, Pancherz H. Effective TMJ and chin position changes in class II treatment: Orthodontics versus orthopedics. Angle Orthod 2008; 78: 813-818

Scapino RP, Canham PB, Finlay HM, Mills DK. The behaviour of collagen fibres in stress relaxation and stress distribution in the jaw-joint disc of rabbits. Arch Oral Biol 1996; 41: 1039-1052

Singh M, Detamore MS. Tensile properties of the mandibular condylar cartilage. J Biomech Eng 2008; 130: 1–7

Soltz MA, Ateshian GA. Experimental verification and theoretical prediction of cartilage interstitial fluid pressurization at an impermeable contact interface in confined compression. J Biomech 1998; 31: 927–934

Smith DM, McLachlan KR, McCall WD. A Numerical Model of Temporomandibular Joint Loading. J Dent Res 1986; 65: 1046-1052

Stegenga B, de Bont LG, Boering G, van Willigen JD. Tissue responses to degenerative changes in the temporomandibular joint: a review. J Oral Maxillofac Surg 1991; 49: 1079-1088

Sun M, Yang J, Zhou R, Li N, Xia J, Gu F. Mechanical analysis on individualized finite element of temporal-mandibular joint under overlarge jaw opening status. Int J Clin Exp Med 2015; 8: 9046-9054

Tanaka E, Tanne K, Sakuda M. A three-dimensional finite element model of the mandible including the TMJ and its application to stress analysis in the TMJ during clenching. Medical engineering & physics 1994; 16: 316-322

Tanaka E, Hanaoka K, van Eijden T, Tanaka M, Watanabe M, Nishi M, Kawai N, Murata H, Hamada T, Tanne K. Dynamic shear properties of the temporomandibular joint disc. J Dent Res 2003; 82: 228–231

Tanaka E, Kawai N, Hanaoka K et al. Shear properties of the temporomandibular joint disc in relation to compressive and shear strain. J Dent Res 2004; 83: 476–479

Tanaka E, Detamore MS, Mercuri LG. Degenerative disorders of the Temporomandibular joint: etiology, diagnosis, and treatment. J Dent Res 2008; 87: 296-307

Tanaka, E, Hirose, M, Inubushi, T, Koolstra, JH, van Eijden, TM, Suekawa, Y, Fujita, R, Tanaka, M, Tanne, K. Effect of hyperactivity of the lateral pterygoid muscle on the temporomandibular joint disk. J Biomech Eng 2007; 129: 890-897

Tanaka E, Koolstra JH. Biomechanics of the temporomandibular joint. J Dent Res 2008; 87: 989–991

Tanaka E, Rego EB, Iwabuchi Y, Inubushi, T, Koolstra, JH, van Eijden, TMGJ, Kawai, N, Kudo, Y, Takata, T, Tanne, K. Biomechanical response of condylar cartilage-on-bone to dynamic shear. J Biomed Mater Res - Part A 2008; 85: 127-132

Tanaka E, Yamano E, Dalla-Bona DA, Watanabe M, Inubushi T, Shirakura M, Sano R, Takahashi K, van Eijden T, Tanne K. Dynamic Compressive Properties of the Mandibular Condylar Cartilage. J Dent Res 2006; 85: 571-575

Throckmorton GS, Dechow PC. In vitro strain measurements in the condylar process of the human mandible. Arch Oral Biol 1994; 39:853-867

Throckmorton GS, Throckmorton LS. Quantitative calculations of temporomandibular joint reaction forces—I. The importance of the magnitude of the jaw muscle forces. J Biomech 1985; 18: 445-452

Tingey EMK, Buschang PH, Throckmorton GS. Mandibular rest position: A reliable position influenced by head support and body posture. Am J Orthod Dentofac Orthop 2001; 120: 614-622

Tuijt M, Koolstra JH, Lobbezoo F, Naeije M. Differences in loading of the temporomandibular joint during opening and closing of the jaw. J. Biomech 2010; 43: 1048–1054

Valesan LF, Da-Cas CD, Réus JC, Denardin ACS, Garanhani RR, Bonotto D, Januzzi E, de Souza BDM. Prevalence of temporomandibular joint disorders: a systematic review and meta-analysis. Clin Oral Investig 2021; 25: 441–453

Vallabh R, Zhang J, Fernandez J, Dimitroulis G, Ackland DC. The morphology of the human mandible: A computational modelling study. Biomech Model Mechanobiol 2020; 19: 1187-1202

Vilimek M. Musculotendon forces derived by different muscle models. Acta Bioeng Biomech 2007; 9: 41–47

Visscher, CM, Huddleston Slater, JJR, Lobbezoo, F, Naeije, M. Kinematics of the human mandible for different head postures. J Oral Rehabil 2000; 27: 299-305.

Wan C, Hao Z, Wen S. The finite element analysis of three grafts in the anterior cruciate ligament reconstruction. Proc - 2011 4th Int Conf Biomed Eng Informatics, BMEI 2011 2011; 3: 1338-1342

Wang L, Lazebnik M, Detamore MS. Hyaline cartilage cells outperform mandibular condylar cartilage cells in a TMJ fibrocartilage tissue engineering application. Osteoarthritis Cartilage 2009; 17: 346-353

Weiss JA, Gardiner JC. Computational modeling of ligament mechanics. Crit Rev Biomed Eng 2001; 29: 303-371

Winters JM, Stark L. Muscle models: What is gained and what is lost by varying model complexity. Biol Cybern 1987; 55: 403-420

Wyatt, WE. Preventing adverse effects on the temporomandibular joint through orthodontic treatment. Am J Orthod Dentofacial Orthop 1987; 91: 493-499

Xu Y, Wu T, Chen Y, Zhang Z. Regulation of the response of the adult rat condyle to intermaxillary asymmetric force by the rankl-opg system. Angle Orthod 2009; 79: 646-651

10. Acknowledgments

My special thanks to Prof. Dr. rer. nat. Christoph Bourauel, Oral Technology, University Hospital of Bonn for giving me the opportunity to pursue my doctoral study in Germany, which was a precious experience at both the academic and the personal levels. His office was always open for our questions and concerns, and he always replied fast and delightfully. It is such a fortune to have him as my professor.

My gratefulness to Dr. rer. nat. Ludger Keilig for his tremendous help, patience, and guidance during my whole study. I would like to thank him for always encouraging me to develop my own research ideas and to practice them freely, which helped me to think and investigate independently.

I would also like to thank PD Dr. rer. nat. Dr. med. dent. Istabak Dörsam for her help in the early beginning of my study. Thanks for her kindness and gentleness, a shy person like me never felt nervous when asking her for help.

I would like to thank Prof. Dr. Yongming Li, Professor of the Affiliated Stomatology Hospital of Tongji University, for inspiring me the theme of this study.

My deep appreciation to Dr. Benedikt Sagl from Medical University of Vienna for sharing his experience during the developing of the FE model.

Moreover, I would like to acknowledge and thank my colleagues and friends for their caring and support, especially Dr. Lamia Singer and Dr. Mathias Hochgerner, for their meticulous proofreading of my thesis.

I would like to acknowledge the China Scholarship Council for the financial support.

Lastly, my genuine thankfulness to my parents for their endless love and support that was always the motivation to never give up and to chase my goal. Without them I wouldn’t be able to successfully finish my study.